1 Introduction

Most bone diseases pose serious health problems and directly impact on a patient's life-long mobility, activity and quality of life. Normally, a bone graft or implant is required There are a large number of bone implant operations occurring each year already. For example, at least a million procedures are carried out worldwide annually (Tanner E and Orr J, 2004). The most desirable implants are those which are autogenous and allogenic i.e. natural materials with no immune rejection. However, sufficient material cannot always be derived from the patient or a suitable donor and current medical technologies are not yet able to synthesize these materials. As a consequence, artificial materials are substituted. Such metals are widely used due to their excellent bulk properties. However, these materials experience significant problems when implanted. They bond poorly to living bones, resulting in slippage when stressed. This is the prime cause of pain following implantation. Furthermore, they are not bioactive. Consequently, the body often rejects the implant. This can lead to inflammation and encapsulation of the implant in fibrous tissue.

Recently, biocompatible coatings have been developed for artificial implants. Among these, crystalline HA is the most widely used. HA is one of the numerous a calcium-phosphate apatite minerals, $Ca_{10}(PO_4)_6(OH)_2$. Its crystal phase possesses a similar structure to that of natural bones. Ideally, the crystalline HA coating has a rough surface so that natural bone in contact with the coating can grow into the interstices. This facilitates integration or osseointegration of the implant into the surrounding bone material, thereby preventing slippage. As well, HA is a bioactive thereby minimizing any problem with rejection.

A variety of techniques has been developed for preparing HA coatings for implants. These include plasma spraying, vacuum deposition, sol-gel and dip coating, and electrolytic processes. Unfortunately, the layer produced by these processes is not crystalline. Subsequently, heat treatment of the HA-coated implant is required (at high temperatures > 700 °C) to crystallize the HA into the required form. Unfortunately, such treatment often generates cracks in the HA coating resulting from differential expansion between the coating and substrate. These cracks substantially decrease the implant's bonding ability to natural bones thereby increasing the likelihood of slippage.

Alternative coating methods are presently under development to overcome this problem. These methods rely on biomimetic techniques, which are designed to directly form a crystalline HA layer in a manner similar to the process of natural bone formation in a human body.

A promising biomimetic technique exploits self-assembling mono-layers (SAMs). SAMs provide a template on the implant substrate to permit the growth of crystalline HA coating. Previous work confirms that crystalline HA coatings can be successfully prepared with SAMs immersed in a simulated body fluid (SBF). However, several weeks are required for formation of the coating layers. This period is excessive and the current process is uneconomic. The goal of the present project was to establish if it was possible to accelerate the rate of the HA coatings formation on bone implants by using SAMs. This goal may be achieved by utilizing alternative SAMs or by varying the nature and conditions of the simulated body fluid to enhance crystal growth. The *in-vitro* performance of the HA coatings was also determined using human-bone, cell-culture experiments.

The research was performed at the School of Chemical Engineering at The University of Adelaide, the Ian Wark Research Institute at The University of South Australia and the Hanson Institute of The Royal Adelaide Hospital.

2 Literature Review

This review will primarily focus on background knowledge relating to bone implants, previous coating methods, biomimetic coating techniques and the results of previous bioactivity studies**.**

2.1 Composition and Structure of Natural Bones

Bones have been widely studied for medical purposes. Their composition and structure is now well understood. Copstead and Banasik (1995) describe bone as a combination of two sorts of materials: organic and inorganic. Moreover, 90%-95% of the organic component is collagen whilst the inorganic components are minerals principally composed of calcium and phosphate. At the cellular level, bone consists of fibroblasts, fibrocytes, osteoblasts, osteocytes, osteoclasts and osteoprogenitors.

Fibroblasts and fibrocytes are responsible for collagen formation to enhance the bone's tensile strength. Osteocytes are mature bone cells. They are sensitive to pressure and enable bone to remodel itself in response to forces or loads. Osteoblasts and osteoclasts lie close to the bone's surface. Osteoblasts work as a matrix. Osteoclasts are responsible for bone resorption. Each of these cells work in concert to control the bone's remodeling, growth and healing processes, and where and how the osteocytes will form (Pritchard, 1979).

The mineral components of a bone, principally calcium and phosphate, account for 65%-75% of dry weight of the bone and constitute the solid part of the bone. They are known as "bio-HA", a kind of calcium phosphate salt with a composition close to that of the mineral HA. The Ca/P ratio varies between 1.5-1.65 depending on bone location (Suchanek and Yoshimuria, 1998).

Human bones are divided into two types depending on their structural differences (Figure 2.1): cortical bones (compact bone) and trabecular bones (spongy bone). Cortical bone is much denser than trabecular bone.

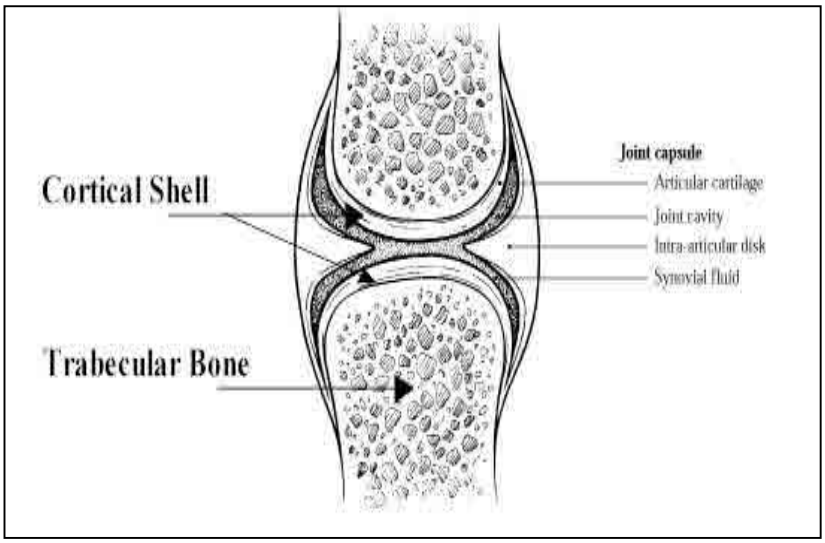

Figure 2.1: Illustration of a cortical shell around a generic long bone joint. (Reproduced from the Michigan University web site, www.engin.umich.edu)

Cortical (or compact) bone is composed of many layers. The inner layer is a matrix made of small collagen fibers and is covered with crystalline HA. These crystals are plate or needle shapes. The fibres with HA form a pipe-like structure called lamella. Many lamellae of different diameters form a concentric structure with an empty middle. This is known as the Haversian Canal. The Haversian Canal permits the transport of blood vessels, nutrients and mineral materials. The concentric structure including the Haversian Canal has been named an Osteon (Figures 2.2 and 2.3). (Suchanek and Yoshimuria, 1998).

In contrast, the trabecular (or spongy) bone is composed of a sponge-like tissue known as trabeculae (Figure 2.4). This kind of bone forms the inner area of the bone. Its porous structure is suitable for the transport and maintain of blood, nutrients and mineral materials (Suchanek and Yoshimuria, 1998).

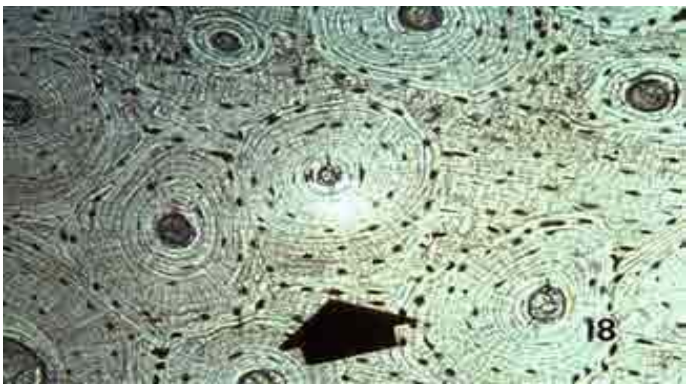

Figure 2.2: Cross section of osteonal cortical bone. (Reproduced from the Michigan University web site)

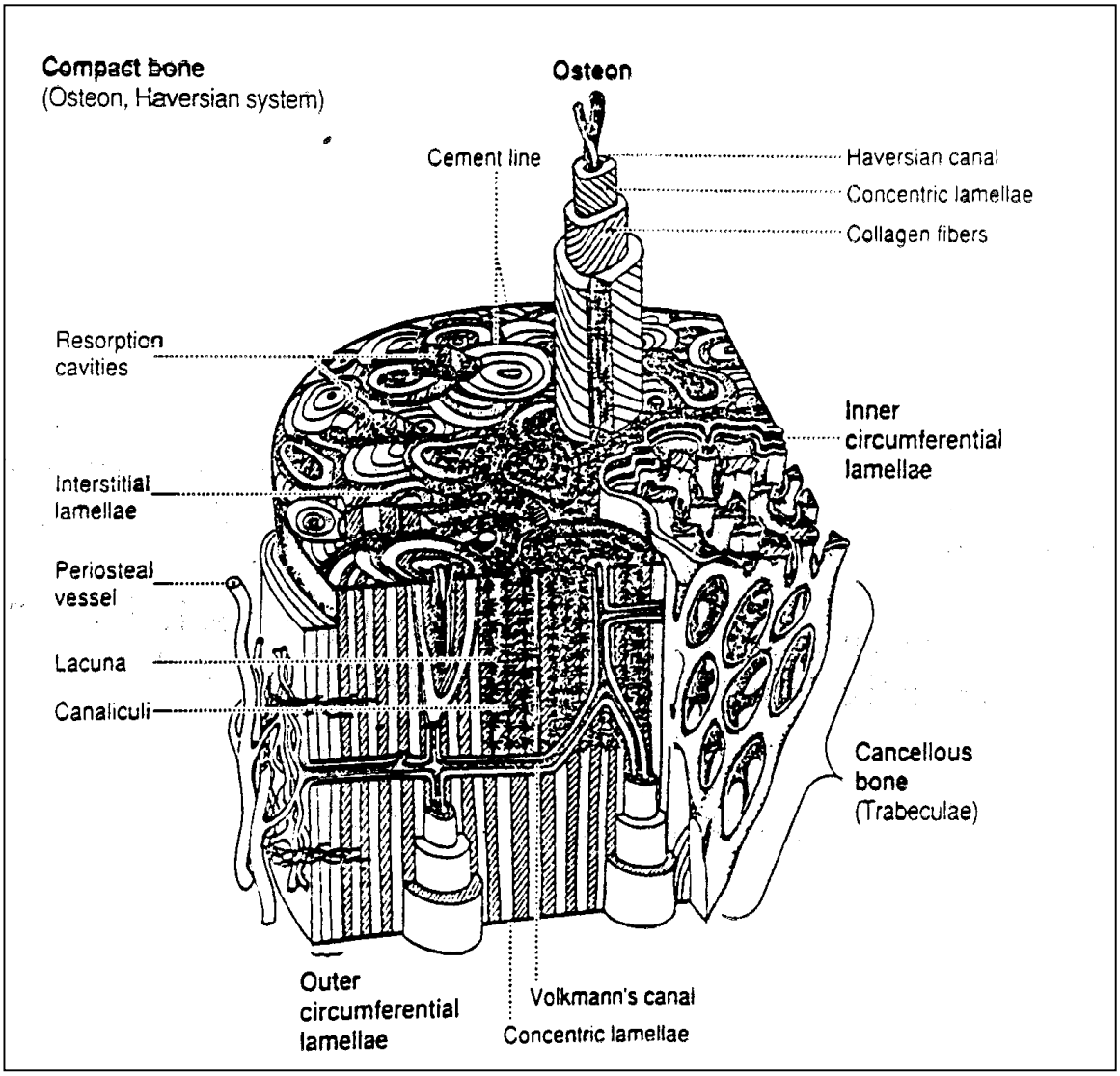

Figure 2.3: Hierarchical levels of structural organization in a human long bone. (Reproduced from the Michigan University web site)

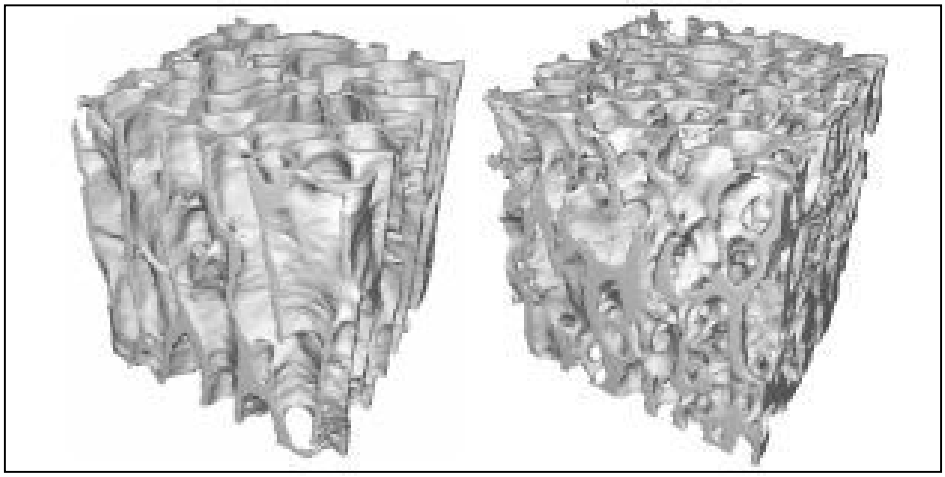

Figure 2.4: Illustration of trabeculae. (Reproduced from the Michigan University web site)

2.2 Background of Implants

Every year, millions of people undergo osteal implant surgery. In the development of this surgical procedure, three implant techniques are used: autograft, allograft and artificial device graft (Vaccaro et al., 2002).

Autograft involves the collection of tissue (e.g. bone) from one part of the patient's body. After culturing the tissue in a nutritious solution and reshaping, this tissue is implanted. Basically, autograft is the safest of the above techniques as rejection problems are avoided. Unfortunately, autograft is only suitable for small implants such as finger junctions or nose bone transplants. However, approximately twenty percent of patients who undergo autograft surgery suffer from infection and experience pain at the implant site (Vaccaro et al., 2002).

Allograft involves collection of tissue from a donor. This tissue is then transplanted into the patient. The key constraint on this technique is location of a suitable donor prior to the allograft. Unfortunately, it is normally very difficult to find a compatible donor. This constraint limits the application of the allograft technique.

Artificial-device grafts involve implantation of artificial materials rather than natural tissue into a patient's body. In contrast to the previous methods, abundant resources are available to produce artificial replacements. Consequently, this technique has become increasingly popular.

2.3 Artificial Implant Materials

Initial studies of artificial implant materials involved titanium metal and its alloy due to their attractive mechanical properties. However, problems were encountered as the materials were not “bioactive” or “biocompatible”. Consequently, natural tissues failed to adhere to the implants. As a result, the implanted devices became encapsulated by fibrous tissues and isolated from the surrounding environment. This phenomenon results in post implant complications and/or eventual failure of most titanium implants (Hench et al., 1984). Since these initial failures, substantial resources have been committed to overcome this problem.

Recently, several new materials have been discovered with good bioactivity and the ability to directly bond to natural bone. These are known as “bioactive ceramics” and include: bioglass (SiO_2-CaO), sintered HA and sintered tri-calcium phosphate (TCP) (Kokubo, 1996). Following observation of the behavior of these bioactive ceramics *in-vivo*, it was determined that the essential requirement for bonding is the formation of a bone-like apatite layer on their surface (Hench, 1981).

The bone-like apatite layer had been characterized as nano-crystalline carbonate apatite (CAP) (Kitsugi et al., 1990). This is similar to the mineral phase in human bones. The mechanism of the binding between bones and the bone-like apatite layer has been described by Loty et al. (2000) as follows. The osteoblast cells proliferate on the bone-like apatite layers, and form a biological matrix containing bio-apatite and collagen whilst consuming the apatite in the bone-like apatite layer and then remodeling the layer. This bonding process between artificial materials and natural bone is identical to that involved in the bonding between natural bones.

The mechanisms of the bone-like apatite layer formation on bio-glass and HA differ. The mechanism of the apatite layer formed on bio-glass was determined by Kokubo (1996) as follows. The calcium ions released from the bio-glass increased the ionic product (IP) of the surrounding solution. The body fluid is already supersaturated with respect to HA. Apatite nuclei will form repidly on the hydrated silica located on the surface of bio-glass. A bone-like apatite layer grows from these apatite nuclei by consuming the calcium, phosphate and a small amount of carbonate ions from the

human body fluid. By contrast, the formation of bone-like apatite on HA occurs due to ion-exchange. The phosphate or hydroxyl ions in HA are exchanged with carbonate ions in human body fluid, however the final composition of the layer is similar to that of the apatite layer formed on bio-glass (Zhang et al., 2003).

Although the bioactive ceramics display excellent *in-vivo* performance, their mechanical properties are problematic. These materials are both fragile and highly elastic. Clearly, a concept with potential would be to couple the bioactivity of bioactive ceramics with titanium's mechanical properties by using titanium metal or its alloys. As a result, HA coatings on titanium metal implants have been widely studied, as their composition is extremely close to that of human bones. This combination has significant potential to improve the implant's bio-acceptability.

2.4 Hydroxyapatite Coatings

HA coatings formed on metal implant materials, primarily titanium and its alloy, rapidly integrate with the surrounding tissues to form a strong bond. Consequently, the capsule-structured tissues that normally form around metal implants are eliminated (Cook et al., 1996). These coatings have been applied in orthopedics since the beginning of the 1980s. However, HA coated implants do exhibit drawbacks. These include a high dissolution rate (Radin and Ducheyne, 1992), low bonding strength between the HA coating and the metal substrates, and low fracture strength (Lacefield, 1994). Clearly, any coating with high dissolution rate will be rapidly solubilized by the body fluid after implantation. As a consequence, the implant becomes loose and unstable. This problem is caused by impurities in the chemical composition of the coating or by low crystallinty of the coatings (LeGeros, 1993). The low bonding strength between the HA coatings and the metal substrates and the low fracture strength caused by cracks in the coatings often restricts the application of HA coated implants to non load-bearing areas. Obviously, the properties of the HA coatings strongly influence the successes of the implant surgery.

As mentioned above, purity and crystallinity affect the dissolution rate of the coating. Unfortunately, a decrease in purity results from the high-temperature treatment process which was designed to develop highly crystalline coatings. This problem can not be avoided in most conventional HA coating techniques to be discussed in the next section with the exception of biomimetic methods. The reason is that the HA coatings made by

these methods are amorphous, and hence, dissolve at an extremely high rate. Consequently, to improve the crystallinity of the coatings, high-temperature sintering is necessary. However, during this process, the chemical composition of the HA coating changes. New phases appear in the coatings due to thermal rearrangement. These include: α-TCP (α-$Ca_3(PO_4)_2$), β-TCP (β-$Ca_3(PO_4)_2$), ACP (amorphous HA), TTCP ($Ca_4P_2O_9$) and OHA ($Ca_{10}(PO_4)_6(OH)_{2-2x}(O)_x(V)_x$) (Sun et al., 2001). The presence of these phases decreases coating purity and affects its long-term stability as these phases are more soluble than crystalline HA. To minimize this problem, the chemical purity of HA coatings must controlled to be in excess of 90%. This recommendation is normally followed by manufacturers.

It has been reported that bone growth is faster on amorphous HA coatings as a consequence of the quicker release of calcium ions. These increase the degree of supersaturation of the surrounding body fluid and improve biomineralization (Weng et al., 1997). Unfortunately, the rapid dissolution rate of such HA coatings still results in poor implants. Therefore, in term of long-term stability, the degree of crystallinity of the HA coatings must be maximized.

Other important HA coating properties include roughness, thickness and structural properties. Very rough coating surfaces normally improve the growth of bones and assist in forming an inter-connected structure thereby improving the adhesion of bone cells to the surface (Tsui et al., 1998). The optimal surface roughness has been little studied and it depends strongly on the implant's location.

The thickness of the HA coating significantly influences an implant's long-term stability. For example, the average sorption rate of a HA coating containing amorphous phases made by plasma spraying is roughly 8-10 μm/y. Therefore, at least 50 μm should be deposited when manufacturing implant devices (Sun et al., 2001). However, an excessively thick coating is not always superior. Geesink et al. (1987) reported that coating thickness exceeding 100 μm significantly increased the risk of fatigue failure. Kukobo (1996) recommended that the normal thickness for a highly crystalline HA coating is approximately 10 μm. The lifetime of such a coating is attractive as the resorption rate is very low whilst the bonding strength between the coating and substrate is high. At present, such coatings are not used surgically and it is difficult to judge the optimal thickness.

Finally, HA coating properties depend on coating methods and the preparation parameters. Current HA coating methods include plasma spray, sol-gel, electron-beam deposition, hot isostatic pressing and biomimetic techniques. Their advantages and disadvantages will be discussed in the next section.

2.5 Current HA Coating Methods

Current commercial HA coating methods, primarily plasma spray, sol-gel, electron-beam deposition and hot isostatic pressing, require subsequent high-temperature heat-treatment to achieve the desired high level of crystallinity. Each technique has disadvantages but they all are used commercially as no problem-free method exists.

Plasma spraying is the most popular commercial method. It is simple with low equipment costs. This method uses ionized plasmas to transport HA particles. These particles are sprayed onto the substrate surfaces forming a coat. The coating made by this method is uniform in macrostructure and this method is economic. However, the plasma spray process is restricted by its line-of-sight property and the low percentage of crystalline phase. The coating is largely amorphous. This amorphous phase dissolves in water and is the prime reason for instability of the HA coating over time. To produce a highly crystalline state, heat treatment is necessary. Unfortunately, this reduces the bonding strength between the substrates and HA coating significantly due to the formation of cracks within the coatings. These stresses result from a mismatch between the thermal properties of the implant and coating (Lacefield, 1994). Moreover, the HA coating made by this method is not uniform in microstructure and chemical composition. The extremely high temperatures reached in the plasma spray generate a mix of crystals: stoichiometric HA, oxyhydroxyapatite (OHA), tricalcium phosphate (TCP) and tetra calcium phosphate (TTCP) (Zhang et al., 2003). Yan et al. (2003) found that the quality of HA coatings made by plasma spray degraded at the inner face. The reason is that HA powder can not be mixed uniformly and cooling process produces several amorphous phases with high dissolution rate. A further drawback is the line-of-sight constraint which limits this method to the implants with simple geometry and surface structure.

Ion beam deposition (Ong et al., 1992) and electron-beam deposition (Choi et al., 1999) use ion beams or electron beams to fix the HA powder onto the surface of the Ti

substrate. The mechanisms of these two techniques are similar. High energy currents increase the state energy of the substrate and narrow the energy gap required to form a chemical bond between the coating and substrate. Both methods form a higher purity coat compared with the plasma spray and also achieve a high bonding strength, (> 30 MPa). However, they are not widely applied commercially. The resulting coat is highly amorphous and rate of generation of the coat is slow. A coating of 700 nm thickness will dissolve in SBF within 8 hours if further heat treatment is not applied (Choi et al., 1999). The major limitation of this method remains its prohibitive cost.

Sol-gel is a wet chemical method. The significant advantage of this method is that it is not restricted to line of sight. Hence, the method is useful for porous surfaces and surfaces with complex geometry. Filiaggi (1996) first applied the sol-gel technique in HA coating preparation. The process involves putting the metal substrate into a sol-gel solution and drawing it out at an appropriate speed to create a dense and uniform coating. Due to the highly amorphous nature of the produced coating, subsequent heat treatment is required at 800°C. This temperature generates cracks in the coatings. Gan and Pilliar (2004) developed an alternative sol-gel method using organic solvents. The traditional sol-gel utilizes an inorganic method. In this method, calcium nitrate tetrahydrate and ammonium dihydrogen phosphate provide the calcium and phosphate sources while calcium nitrate tetrahydrate and triethyl phosphate are used in organic method. The organic coating method produced a more uniform coat than that made by the inorganic method (Figure 2.5).

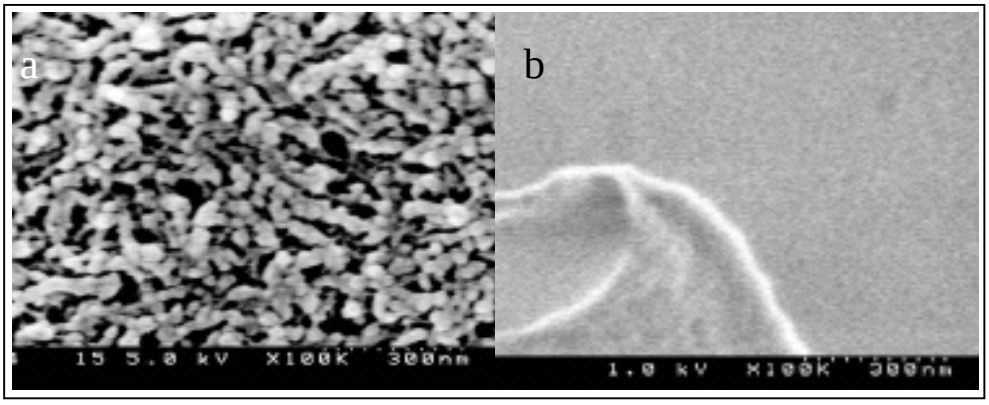

Figure 2.5: (a) SEM images of inorganic sol-gel method formed HA coating; (b) SEM images of organic sol-gel method formed HA coating (Gan and Pilliar, 2004).

As well, the organic sol-gel method has other advantages: relatively low operating temperatures and crack-free products with high bonding strength. The operating

temperature is reduced to about 500°C. This is much lower than that of traditional sol-gel method (Filiaggi, 1996). The lower temperature results in the formation of crack-free coatings. The thickness of the coating made by the organic method is 1.5 μm which is almost twice that produced by the traditional method. The organic method also improved the bonding strength to 50 MPa. The reason for this improvement was discovered using TEM. The coatings were bonded to the Ti substrates by chemical reaction (Gan and Pilliar, 2004).

$$2Ca_{10}(PO_4)_6(OH)_2 + 4TiO_4 \rightarrow 6Ca_3(PO_4)_2 + 2CaTiO_5 + 2H_2O \qquad \textbf{(2-1)}$$

Unfortunately, the organically formed coatings were plagued by low crystallinity.

Another advanced sol-gel method was developed by Kim et al. (2004). Their idea was to use a TiO_2 layer as a bridging layer between the HA coating and titanium substrate. This titania layer improves the chemical affinity both between HA/TiO_2 and TiO_2/Ti. As well, the TiO_2 layer reduced the thermal property mismatch between the HA coating and titanium substrate as the thermal expansion coefficient of TiO_2 lies between that of titanium and HA. Bonding strength was improved from 30 MPa (without TiO_2 layer) to 55MPa. Unfortunately, the HA coating constructed using this method dissolved completely and rapidly in an *in-vivo* environment. To date, all sol-gel applications appear to have been proven unsuccessful.

Hot isostatic pressing is a method that uses high temperature and pressure to produce a uniform HA coating. Initially, the use of hot isostatic pressing for HA coating development was unsuccessful. A problem existed during this process. The hydroxyaptite powder was covered by a gas-tight metal or glass which then reacts with the HA powder at high temperature. This problem was solved by Hero et al. (1994). In their method, boron nitride (BN) powder was inserted between the HA layer and the glass capsule and the hot isostatic-pressing was operated at temperatures up to 850°C at pressures up to 1000 bar. This produced a coating with uniform structure and texture. However, the resulting chemical purity was not sufficiently high due to heating, and vertical cracks abounded within the coatings. These cracks produced a product with a low bonding strength. To improve the bonding strength, Li et al. (1996) mixed partially-stabilized zirconia and HA powder to form the biocompatible coating. The bonding strength was reported to exceed 600 MPa. This is a significant improvement compared with that of pure HA coatings (55MPa). However, subsequent release of elemental Zn

from this coating may contaminate the surrounding body environment.

In summary, no current technique is problem-free. Most fail to overcome the serious drawback of low crystallinity which necessitates further heat treatment. Clearly, an alternative method is desirable for production of crystalline HA coating on implants. Improved methods should form the layer in a low temperature environment and achieve a high level of crystallization.

2.6 Biomimetic Techniques

Biomimetic HA coating techniques are low temperature techniques based on observations of the natural formation and growth processes in the mineral phase in bones. Organic functional films are formed on the substrate's surfaces to induce the mineralization by apatite crystals. In nature, the formation of a bone's mineral only occurs when heterogeneous nucleation overwhelms homogeneous nucleation. A diagram illustrating the ideal situation is provided in Figure 2.6 (Bunker et al., 1994). Hence, background knowledge of crystallization in aqueous solutions is necessary when understanding and simulating the bone formation process.

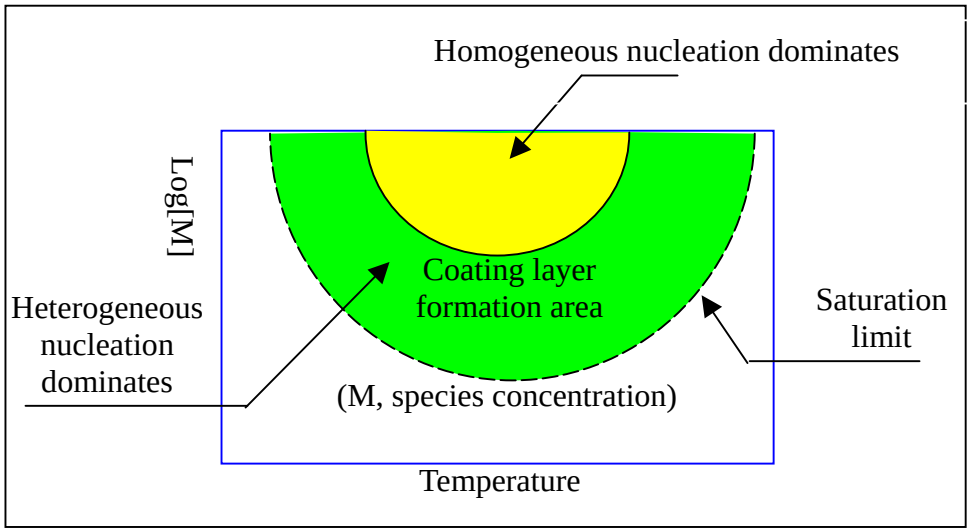

Figure 2.6: Film-forming species dissolved in water.

2.6.1 Crystallization in aqueous solution

Crystal formation in an aqueous solution is controlled by numerous factors, including ion concentration, temperature and saturation degree (Metz, 1976). Work in this area has been reviewed by Kashchiev et al. (2003).

Crystal nucleation and growth are rate processes and require a “driving force”, $\Delta\mu$ (joule/mol), defined as:

$$\Delta\mu = \mu_s - \mu_c \qquad \textbf{(2-2)}$$

Where μ_s is chemical potential of a molecule in solution and μ_c is its chemical potential in crystal phase. The value determines is a solution is supersaturated, undersaturated or saturated ($\Delta\mu$: > 0, < 0 or = 0). Chemical potentials are dependent on temperature (Metz, 1976) and $\Delta\mu$ is given by:

$$\Delta\mu = kT\ln(S) \qquad \textbf{(2-3)}$$

Where k is Boltzmann constant, S is saturation degree and T is absolute temperature. In this form, the saturation degree, S, is defined as:

$$S = (a_1 / a_{1e})^{N_1} (a_2 / a_{2e})^{N_2} \cdots (a_j / a_{je})^{N_j} \qquad \textbf{(2-4)}$$

Where $a_1 \cdots a_j$ are the actual ions activities and $a_{1e} \cdots a_{je}$ are the equilibrium ions activities. In sufficiently dilute solution, a can be replaced by molar concentration, C, hence:

$$S = (C_1 / C_{1e})^{N_1} (C_2 / C_{2e})^{N_2} \cdots (C_j / C_{je})^{N_j} \qquad \textbf{(2-5)}$$

In supersaturated solutions, the driving force exceeds zero but, in some cases, no crystals may form. To explain this phenomenon, it is necessary to consider the crystal formation work, W (joules):

$$W_{(n)} = -n\Delta\mu + \Phi_{(n)} = -nKT\ln S + \Phi_{(n)} \qquad \textbf{(2-6)}$$

Where $W_{(n)}$ is the formation work of a crystal bulk containing n molecules and $\Phi_{(n)}$ represents the excess energy of the crystal cluster, which is defined as:

$$\Phi_{(n)} = \gamma A_{(n)} \qquad \textbf{(2-7)}$$

Where γ is the specific surface energy of crystal/solution interface and $A_{(n)}$ is the crystal surface area. If a solid-liquid interface is involved in the system, the conditions become more complex as more than two phases now exist in the system. This means that more than one interface must be considered, as illustrated in Figure 2.7.

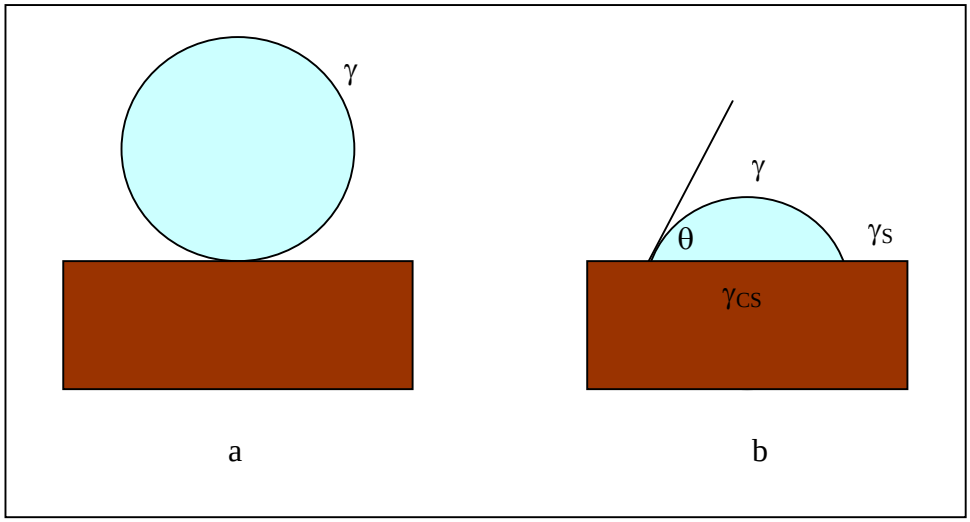

Figure 2.7: Illustration of crystal formed on substrates: (a) homogenous (HO) nucleation (θ = 180°), (b) heterogeneous (HE) nucleation (180° > θ > 0°). [γ, γ_s and γ_{cs} represent the interface energy of crystal/solution, substrate/solution and crystal/substrate, respectively.]

In these cases, equation 2-7 should be revised as

$$\Phi_{(n)} = \left[(1/4)(2+\cos\theta)^2\right]^{1/3}\gamma A_{(n)} \qquad \textbf{(2-8)}$$

From Eq. 2-8, it can be shown that $\Phi_{(n)HO} > \Phi_{(n)HE}$.

The specific surface energy γ is a temperature function (Kashchiev, 2000)

$$\gamma = \left(\beta KT / v^{2/3}\right)\ln\left[1/vC_e(t)\right] \qquad \textbf{(2-9)}$$

Where β is a constant, v is the volume of a crystal molecule and $C_e(T)$ is the equilibrium molecule concentration at absolute temperature T.

Therefore,

$$W_{(n)} = -nKT\ln S + \left[(1/4)(2+\cos\theta)(1-\cos\theta)^2\right]^{1/3}\left(\beta KT / v^{2/3}\right)\ln\left[1/vC_e(t)\right]A_{(n)} \qquad \textbf{(2-10)}$$

From Eq. 2-10, it is clear that crystal formation is controlled by temperature, the degree of saturation and interface energy. Temperature and the degree of saturation are easily controlled. However, interfacial energy depends on surface properties and this is difficult to quantify.

2.6.2 Effects of surface properties and the surface modification

Important surface properties include surface texture, hydrophobicity and electrical

charge. The texture of the surface is important in HA coating formation. A highly organized substrate surface is necessary (Mao et al., 1998). For example, the experiments of Cho et al.(1996) showed that the HA coating was possible on an ordered silica surface while no film formed on a disordered silica surface of the same chemical composition. Generally, hydrophilic surfaces favor HA formation more strongly than hydrophobic surfaces. As well, negatively charged surfaces were reported to have better HA inducing ability than positively charged surfaces (Tanahashi and Matsuda, 1997). A widely accepted explanation is that the HA heterogeneous crystallization in supersaturated solutions is triggered by the adsorption of calcium ions on the surface (Zhu et al., 2004). An organized, hydrophilic and negatively charged surface will be desired for HA coat formation.

The strong influence of surface properties on coating formation means that the key step in any biomimetic method is chemical modification of the surface to achieve the optimal surface properties. Surface modification methods for HA coating formation include both chemical modification and self-assembled monolayer attachment (Bunker et al., 1994).

A range of products have been produced through chemical modification techniques. These include Si-OH, Ti-OH, Zr-OH, Nb-OH and Ta-OH (Kokubo et al., 2003). Hydroxyl functional groups may be produced on bulk surfaces directly and this group could provide promise of good HA inducing ability due to its hydrophilic surface. The method is simple and involves two steps: NaOH treatment and heating. However, other chemical groups such as carboxylic acid and phosphate groups can not be prepared through such simplistic direct chemical modification of the surface (Tanahashi and Matsuda, 1997). To overcome this, SAM techniques have been developed. SAMs can provide surfaces with a range of functional groups and different properties. Another advantage of this technique is that surfaces modified by the SAM are highly organized.

2.6.3 Application of SAMs

SAMs (self-assembled monolayers) are compact and highly organized monolayers formed through chemical adsorption. The structure of a single SAM molecule involves three main elements (Cook et al., 1988): the functional top group, anchor end and an alkyl chain between them (Figure 2.8 b). The anchor end is a chemical functional groups containing electron-rich elements such as S, O and Cl. Affinities between the

anchor functional group and substrate must be sufficiently strong to form a polar covalent or ionic bond (Figure 2.8 c) when the substrate is hydroxylated (Figure 2.8 a).

Many different interactions between SAM molecules and substrates are possible. These include molecules terminated by -trialkyl, -trichloro or trialkoxysilane on hydroxylated Si substrates and alkanethiols SAMs molecules on gold substrates (Smith et al., 2004).

Moreover, Liu et al., (2002) demonstrated that SAM molecules terminated with trichlorosilane may bond with hydroxylated titanium. Common functional top groups for SAM have included -CH_3, -NH_2, -OH, -SH, -SO_3H, -COOH, –PO_4H_2. The following reviews the application of SAMs relevant to HA formation on titanium.

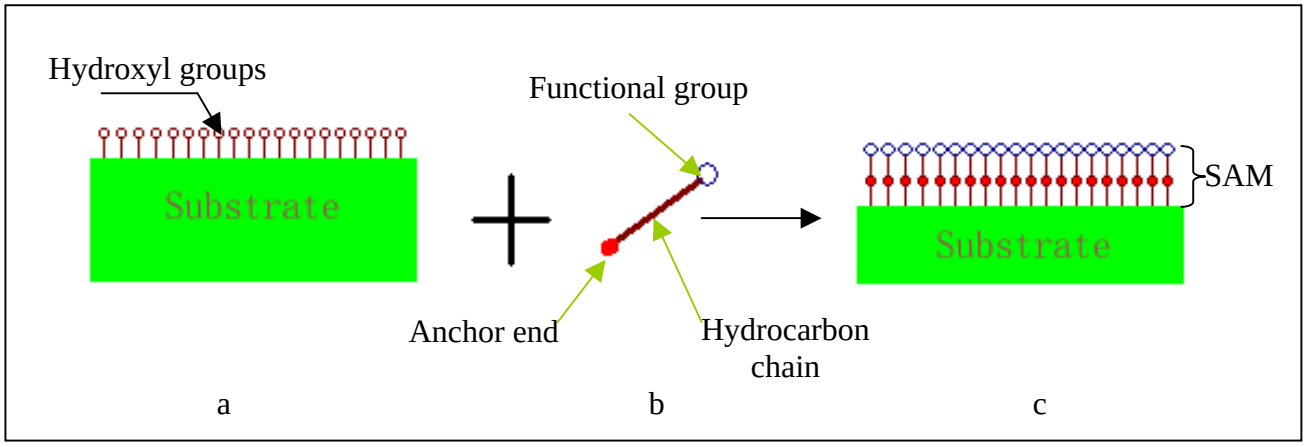

Figure 2.8: Illustration of SAM formation.

Campbell et al. (1996) investigated HA formation on a titanium alloy. SAMs with an alkyl organic spacer, silane-coupling agent and sulfonic acid (–SO_3H) end group have been used. Coatings of 5-10 μm developed after several days' immersion in a simulated body fluid (SBF). Composition and mineral characteristics were consistent with crystalline HA. Using a slightly different organic spacer with an identical coupling agent, Mao et al. (1998) studied HA coatings formed on titanium surfaces using a SAM containing both carboxyl (–COOH) and hydroxyl (–OH) end groups. After seven days in a supersaturated solution (composition undefined), a 40 μm layer of crystalline HA was obtained. Liu et al. (2002) produced a range of alkyl-based SAMs on titanium foil, each containing different end groups: –OH, –COOH, phosphate (–PO_4H_2) and vinyl (–$CH=CH_2$). Crystalline HA formation was successfully obtained with –PO_4H_2 and –COOH, but not –OH & –$CH=CH_2$. The nucleating ability of –PO_4H_2 was concluded to be greater than –COOH.

These studies suggest that the functionalized end groups most suited for HA formation using a SAMs on a titanium implant surface are $–SO_3H$, $–PO_4H_2$ or –COOH. However, previously reported performances of these functional end groups cannot be effectively compared as SAM preparation methods and experimental conditions for HA formation were different. Furthermore, a study without SAMs on titanium (Kokubo et al., 2003) and one with SAMs on gold surfaces (Tanahashi & Matsuda, 1997) suggest that the –OH functional groups can induce HA nucleation. This contradicts the experimental results obtained by Liu et al. (2002). In this project, work was undertaken to verify the results of earlier studies and then to compare the performance of a diverse range of functionalized end groups including –OH, $–SO_3H$, $–PO_4H_2$ and –COOH for HA formation on titanium with SAMs in SBF.

2.7 Previous Studies of Cell Behaviour on Biomaterials

Osteoblast and osteoclast cells are normally used in studies aimed at osteopeadic applications. The behaviour of osteoblast cells was determined by observing the number of adhering and proliferating cells, the calcium content in cell layers, the expression of genes and mineralization *in-vivo* (Findlay et al., 2004). By contrast, the behavior of osteoclast cells is normally quantified by the substrate's resorption level (Dio et al., 1999).

There are few studies of cell behaviors involving titanium or apatite. Findlay et al. (2004) reported that titanium did not show an outstanding ability for culturing human osteoblast-like cells compared with Co-Cr and glass-ceramics. Okumura et al. (2001) demonstrated HA's *in-vivo* performance is better than that of titanium. Dio et al. (1999) studied rabbit osteoclastic cell behaviour on various calcium phosphates including HA, β-tricalcium phosphate (β-TCP), carbonate apatite (CA), tetracalcium phosphate (Te-CP), α-tricalcium phosphate (α-TCP), dicalcium phosphate dihydrate (DCPD), and octacalcium phosphate (OCP). They found crystalline carbonated apatite was the only substrate that allowed osteoclastic cells to resorb. Moreover, Leeuwenburgh et al. (2001) found that crystalline carbonated calcium phosphate clearly exhibited absorption by mouse osteoclastic cells. As HA, especially crystal carbonated HA, appears to have a promising in-vivo performance, it is reasonable to resume that HA coating could improve the bio-conductivity of the titanium implants. Unfortunately, such researches

are still missing. Therefore, studies of the human cells growth and behaviour on HA coated titanium were performed.

2.8 Aims

The goal of this study is to identify the end group possessing the best nucleating ability for the growth of crystalline HA coating. However, the formation of HA coating on titanium is a complex process. Many significant variables influence performance: SAM type, temperature, pH, ion concentrations and Ca/P ratio. In this project, the effects of various factors and their interactions in HA coat formation, growth and chemical composition are quantified. Acceleration of HA formation was investigated by a two-level fractional factorial design experiment. Finally, interactions between HA coated titanium and human cells was studied from the behavior of human bone osteoblast cells on titanium metal coated with crystalline HA using a carboxylic acid SAM.

3 Experimental Procedures

3.1 Introduction

The growth and nature of HA coatings produced by SAMs techniques have been widely studied on gold (Tanahashi and Matsuda, 1997) and silicon (Zhu et al., 2003) substrates. These studies demonstrated the clear potential of this methodology and the first step to realize this conception is to form suitable SAMs on titanium substrates.

There are two prototypical systems for anchoring SAMs on a substrate: thiol and silane. Thiol SAMs are usually applied on compositionally stable metals such as gold. However, it is not suitable for titanium because its surface properties are substantially different (Nanci et al., 1998). Titanium metal is normally covered by an oxidized layer. Silane SAMs have been successfully used on oxidized silicon. There is no significant difference in chemical functionality of oxidized titanium and oxidized silicon. Therefore silane SAMs was selected.

In this project, four types of silane SAMs were prepared on titanium substrates. They were -OH, -SO_3H, -COOH and –PO_4H_2 SAMs. As well, hydroxylated titanium metal was also studied as control. The SAM layers were prepared by titanium silanization and SAM functionalization. Two sorts of alkylanesilane molecules were used: 7-octenyltrichlorosilane (OTES) and (3-Mercaptopropyl)-trimethoxysilane (MPTMS). Titanium silanization was performed by immersing hydroxylated titanium wafers in alkylanesilane solutions prepared from the two alkylanesilane molecules separately. The functionalization was undertaken by converting the functional groups at the top of the SAM molecules through chemical reactions. Details are shown in Figure 3.1.

The characterization of these SAMs was performed using water contact-angle measurement (WCAM) and time of flight-secondary ions mass spectroscopy (TOF-SIMS). WCAM is a simple but efficient analysis technique. It has been widely used to recognize SAMs (Martins et al., 2003; Barbosa et al., 2004). TOF-SIMS is a powerful surface analysis technique. Cox et al. (2001) used TOF-SIMS to identify several SAMs. However, this did not include the SAMs proposed in this study, where TOF-SIMS was applied to detect P on phosphate SAMs and S on sulfonic acid SAMs. The confirmation of -OH and -COOH SAMs by TOF-SIMS was based on measurement of the C/O ratio.

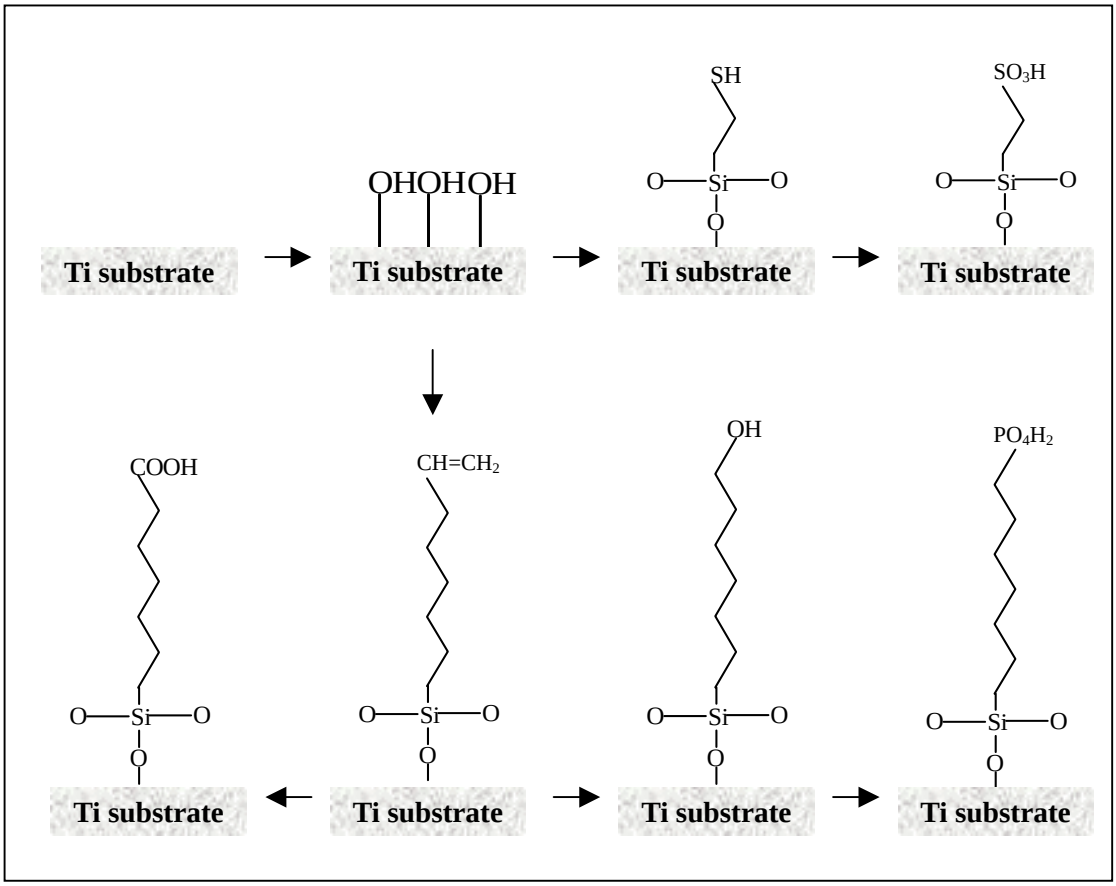

Figure 3.1: Silanization and functionalization processes.

After SAM formation experiments, HA layer formation experiments were performed utilizing the Kokubo method (Kokubo, 1996). In this method, HA layer was formed by placing SAM coated Ti wafers in simulated body fluid containing similar ion concentrations to those of human blood plasma. Tanahashi and Matsuda's research (1997) on gold substrates has proved that this method works for many negatively charged SAMs. Fourier transform infrared spectroscopy (FTIR), energy dispersive x-ray spectrometery (EDS), X-ray diffraction (XRD) and scanning electric microscopy (SEM) were employed to analyze the resulting HA coatings.

Although the effects on HA crystal formation have been studied, most works (e.g. Kim et al., 1999) were focused only on the effects of changes in ionic concentrations on HA formation. To date, little work has been performed to quantify the effects of other factors, such as temperature and pH; moreover, the combined effects of several factors have not been systematically studied. In this study, the effects of ion concentration, pH, temperature and their combined effects were inspected. However, if all the combinations were considered and replicated twice, then 32 runs were required. This

number of experiments was too large for a screening study. Therefore, one-half two-level fractional factorial design (Montgomery, 2001) was employed to reduce the number of runs to 16. EDS and SEM were employed to compare the chemical composition and surface morphology of the resulting HA coatings.

To quantify the *in-vitro* performance of the resulting products, normal human osteoblast cells culture experiments were conducted. This was performed using similar methods employed for the previous work on tantalum metal by Findlay et al. (2004). Human osteoblast (bone) cells were derived from two individuals. After cell culture, a fixed number of cells were transplanted onto titanium coated with HA and onto titanium metal discs. The cell growth differences were measured by quantifying their mineralisation levels (cell layer-associated calcium ions levels). This value is closely related to the number of the attached cells and likewise measures in some way, the cell's activity.

3.2 Preparation of Titanium Surfaces

Titanium surface preparation involved the following sequence of steps: foil cutting, flattening, microorganism removal, polishing and hydroxylation.

The titanium sheets were 15×15×0.025 cm. These were too large for experimentation (including analysis). Therefore, titanium sheet was cut with an electric cutter to a final specimen size of 1×1×0.025 cm, which was more suitable for most analysis equipment. Some distortion caused by the cutting process could not be avoided and preliminary investigation found this affected the water contact angle measurement results significantly. To solve this problem, the distorted specimens were held under a compressive load of 4000 kPa for 20 minutes, then turned and the process was repeated once. Flattened specimens were cleaned in acetone in ultrasonic bath for 6 minutes then this cleaning process was repeated three times to eliminate the organic materials followed by air drying. The polishing treatment was performed by scraping the surface with delicate task wipes to remove the old oxide layer. A new uniform oxide layer was allowed to form following exposure in air for 30 minutes. Next, specimens were thrice washed in distilled and deionized water.

Previous work on silicon suggests that a chemically pure hydroxyl layer is necessary for

silane formation due to the requirement for a chemical covalent bonding reaction to occur. Hydroxylation was performed by immersing titanium wafers in “piranha” solution: concentrated H_2SO_4 and H_2O_2. Many piranha solutions with different in H_2SO_4/H_2O_2 ratio have been developed for hydroxylation purposes. After study, a piranha solution containing 50% v/v (98% H_2SO_4) and 50% v/v (30% H_2O_2) was chosen. Before hydroxylation, all the glassware was cleaned by piranha solution as the solution is also an effective chemical disinfectant for many organisms. If the glassware was not thoroughly clean, then the remaining organisms would affect the chemical purity of the resulting hydroxyl layer. Titanium wafers were soaked in fresh piranha solution for 10 minutes. The wafers were then washed in deionized water (three times) and air-dried.

3.3 SAM Formation and Functionalization

SAMs were prepared on the hydroxylated Ti wafers to provide five different types of functional end group: $–SO_3H$, $–CH=CH_2$, –OH, –COOH and $–PO_4H_2$. Preparation of the $–CH=CH_2$, –OH, –COOH and $–PO_4H_2$ SAMs followed methods presented by Liu (2002) with slight variations in reagents and their concentrations. The $–SO_3H$ SAM was constructed using a technique developed by Niesson (2001). This SAM possessed a different organic spacer.

The $–SO_3H$ SAM was formed by immersing Ti wafers in an anhydrous toluene with 1 % (v/v) 3-mercaptopropyltrichlorosilane, $HS(CH_2)_3SiCl_3$, contained in a reaction vessel under a N_2 atmosphere. The reaction vessel was sealed and heated at 65 ºC for 5 hrs. Wafers were removed and washed with anhydrous toluene, then with distilled water. Wafers were placed in supersaturated oxone (potassium peroxomonosulfate) solution at room temperature, and then washed with distilled water and air-dried.

The $–CH=CH_2$ SAM was prepared by immersing Ti wafers in anhydrous toluene with 1 % (v/v) 7-octenyltrichlorosilane (OTES), $CH_2=CH(CH_2)_7SiCl_3$, for 5 min at ambient temperature under N_2 atmosphere. Wafers were removed and washed with toluene, and then with distilled water, before being air-dried. The –OH SAM was made from wafers already containing $–CH=CH_2$ SAM. The $–CH=CH_2$ functional group was converted to –OH by hydroboration and oxidation. Wafers were exposed to 1 M B_2H_6 for 30 min. They were then immersed in an equal volume solution of 0.1 M NaOH and 30 % (v/v)

H_2O_2 for 5 min. Wafers were removed and washed with distilled water, then air-dried. Phosphorylation was used to prepare the $–PO_4H_2$ SAM from wafers with –OH SAM. Wafers were placed in anhydrous acetonitrile containing 0.2 M phosphorus oxychloride ($POCl_3$) and 0.2 M 2,4,6-collidine for 1 hr. Wafers were removed and washed with distilled water, then air-dried. The –COOH SAM was also prepared from wafers containing $–CH=CH_2$ SAM. Wafers were immersed for 5 min in 5 % (w/v) $KMnCl_3$ solution, acidified with 0.1 M HCl. Wafers were removed and washed with distilled water, then air-dried.

3.4 Simulated Body Fluid and Hydroxyapatite Layer Formation

Simulated body fluid (SBF) is an artificial solution with ionic concentrations analogous to those of human blood plasma. In this study, it was prepared using a similar recipe to Zhu et al. (2004) by dissolving NaCl (8g), $NaHCO_3$ (0.353g), KCl (0.224g), K_2HPO_4 (0.174g), $MgCl_2.6H_2O$ (0.305g), $CaCl_2$ (0.278g) and Na_2SO_4 (0.071g) into 1L distilled water. The pH was adjusted to 7.4 by adding HCl (0.1 M). The ionic compositions of the SBF compared with blood are shown in Table 3.1.

Table 3.1: Ionic concentrations of blood and SBF (mM).

	Na^+	K^+	Ca^+	Mg^{2+}	Cl^-	HCO_3^-	HPO_4^-	SO_4^{2-}
Blood	142.0	5.0	2.5	1.5	103.0	27.0	1.0	0.5
SBF	142.0	5.0	2.5	1.5	148.8	4.2	1.0	0.5

During factorial experiments, several variants of this recipe were used to produce modified SBF solutions. These were prepared by adjusting one or more components of the standard SBF. Details are provided in section 3.6.

Titanium (test) wafers containing different SAMs and untreated Ti (control) wafers were immersed in SBF in individual glass test tubes. The wafers were suspended vertically (Figure 3.2). This orientation was chosen to prevent settling out on wafers of precipitates from the solution. Sampling was performed at 1, 5, 10 and 30 days after immersion. Only one test wafer for each SAM and one control wafer were set aside for analysis at each sampling time; there was no replication.

Figure 3.2: Wafers placed in SBF in vertical direction.

3.5 Analysis of SAMs and HA Coatings

Wafers containing different SAMs were analyzed using water contact angle measurement and TOF-SIMS to confirm the presence of the desired functional end group. Water contact angle measurements were performed in triplicate. Analysis of the HA coated wafers included FTIR, XRD, SEM and EDS. As some of the analyses were destructive not all could be performed at each sampling time. FTIR spectroscopy was performed on the control and test wafers at 1 and 10 days following immersion in SBF. XRD was performed on the control and test wafers at 20 days. SEM and EDS was conducted on the test and control wafers at 5, 20 and 30 days.

3.5.1 Water contact angle

The static contact angle of water on SAM-coated Ti wafers was measured at 25 ºC using a proprietary contact angle goniometer (Ian Wark Research Institute, Adelaide, Australia) by placing a 10 μl drop of distilled water on the wafer surface. The droplet shape was imaged with a video camera and contact angle calculated by proprietary software (Ian Wark Research Institute, Adelaide, Australia).

3.5.2 TOF-SIMS

TOF-SIMS uses a pulsed primary ion beam to desorb and ionize species from a sample surface. The ionized species are accelerated into a mass spectrometer, where they are

analyzed by measuring their time-of-flight from the sample surface to the detector.

A model TRIFT 2100 spectrometer (Physical Electronics, Minnesota, USA) with Ga liquid metal gun (LMIG) was employed. Flight time and intensity data were automatically recorded and analysed by computer with proprietary software (Ian Wark Research Institute, Adelaide, Australia). The cumulative particle count period during each analysis was 2 min, during which nine separate regions at equidistant locations on a wafer were exposed to the ion beam.

3.5.3 SEM & EDS

Wafers were sputtered with carbon before observation. A Camscan Model CS44FE field emission scanning electron microscope (Obducat Camscan, Cambridgeshire, UK) equipped with Energy Dispersive X-ray spectrometer was employed to investigate surface topography and elemental composition. SEM images were taken from directly overhead. EDS was performed at 15 kV with a 30° take-off angle.

3.5.4 FTIR

A Nicolet Magna-IR 750 spectrometer (Thermo Electron Corporation, Massachusetts, USA) was used to characterize surface chemical functionality. Spectra were collected between 4000 and 400 cm^{-1} at a resolution of 4 cm^{-1}. Background measurements were performed with KBr powder (Sigma-Aldrich, Missouri, USA).

3.5.5 XRD

The crystalline status of surfaces was investigated with a Philips Powder X-ray diffractometer (Philips Analytical, Massachusetts, USA). Cu Kα (λ=0.154 nm) radiation was used for excitation and placed at a distance of 20mm. The scanning speed is $0.02^{o}s^{-1}$.

3.6 Effects of Various Reaction Conditions on HA Coating Formation

The study of various reaction conditions on the formation of the HA coatings was divided into three steps: factor selection, experiment design and data analysis.

3.6.1 Factor Selection

Based on an analysis of work presented in literature review, four key factors were identified. They were (a) calcium ion concentration, (b) Ca/P ratio, (c) pH and (d) temperature.

Kim et al. (1999) have shown the calcium phosphate concentrations of the SBF significantly affect the properties of HA coatings including Ca/P ratio in coatings, growth rate and crystal size. Kokubo (1996) reported that temperature influenced the HA growth rate during a biomimetic layer formation. Finally, Ca/P and pH were reasonably considered to affect the HA formation process. To date, no comprehensive study has compared the relative influences of, and the interactions between, these factors. The levels of the factors were summarized in Table 3.2.

Due to constraints on resources, initial screening experiments were not performed to decide upon the required range of these factors. Individual ranges were determined based on previous studies and the requirement for the solutions to remain supersaturated over the test period.

Table 3.2**:** Factors selected for 2^{4-1} experiment design.

Factors	Levels	values
a: Ca ions con. (mM)	High +	5
	Low -	1.875
b: Ca/P ratio	High +	2.5
	Low -	1.57
c: pH	High +	8.4
	Low -	6.5
d: Temperature (°C)	High +	67
	Low -	18

3.6.2 Experimental design

The data were collected by performing a “one-half two-level fractional factorial experiment” (Montgomery, 2001). The experiment design involves setting two levels for each factor (details are shown in Table 3.2) and inspecting only half of the

combinations (Table 3.3).

Table 3.3: Combinations [variables] used in the 2^{4-1} experiment design.

Combinations [variables]	Solution parameters			
	Ca ion con.	Ca/P ratio	pH	Temperature
1	1.88 mM	1.57	6.5	18°C
ad	5.00 mM	1.57	6.5	67°C
bd	1.88 mM	2.5	6.5	67°C
ab	5.00 mM	2.5	6.5	18°C
cd	1.88 mM	1.57	8.4	67°C
ac	5.00 mM	1.57	8.4	18°C
bc	1.88 mM	2.5	8.4	18°C
abcd	5.00 mM	2.5	8.4	67°C

As previously indicated, SBF was prepared by dissolving NaCl, $NaHCO_3$, KCl, K_2HPO_4, $MgCl_2.6H_2O$, $CaCl_2$ and Na_2SO_4 into distilled water. The pH was adjusted by adding 0.1M HCl and temperature was controlled using a heat plate. The ionic concentrations of various solutions employed for each combination are shown in Table 3.4.

Table 3.4: Ionic concentrations and environmental parameters for various solutions.

Combination	Concentration (mM/L)								pH	T (°C)
	Na^+	K^+	Mg^{2+}	Ca^{2+}	Cl^-	HCO_3^-	HPO_4^{2-}	SO_4^{2-}		
[1]	142	5.39	1.5	1.88	146.75	4.2	1.19	0.5	6.5	18
ad	142	10.63	1.5	5.00	153.00	4.2	3.82	0.5	6.5	67
bd	142	4.50	1.5	1.88	146.75	4.2	0.75	0.5	6.5	67
ab	142	7.00	1.5	5.00	153.00	4.2	2.00	0.5	6.5	18
cd	142	5.39	1.5	1.88	146.75	4.2	1.19	0.5	8.4	67
ac	142	9.37	1.5	5.00	153.00	4.2	3.19	0.5	8.4	18
bc	142	4.50	1.5	1.88	146.75	4.2	0.75	0.5	8.4	18
abcd	142	7.00	1.5	5.00	153.00	4.2	2.00	0.5	8.4	67

All the solutions in Table 3.4 were supersaturated.

-COOH SAMs prepared using the method developed in Chapter 3.2 were employed. The wafers were soaked in the modified SBF solutions and at 5 days the resultant HA coatings were analyzed by EDS for Ca content and Ca/P ratio, the response variables.

3.6.3 Statistical analysis

Two statistical methods were employed to analyze the results: normal probability plot analysis and regression model analysis.

Normal probability plot analysis

The estimated values (L) of the variables were calculated using the set of equations shown below (Montgonery, 2001):

$$L = \frac{1}{n2^{k-2}}(\text{Contrast}) \quad \textbf{(3-1)}$$

And

$$Contrast_a = (\text{ad+ab+ac+abcd-bd-bc-cd-1}) \quad \textbf{(3-2)}$$

$$Contrast_b = (\text{ab+bc+bd+abcd-ac-ad-cd-1}) \quad \textbf{(3-3)}$$

$$Contrast_c = (\text{ac+bc+cd+abcd-ab-ad-bd-1}) \quad \textbf{(3-4)}$$

$$Contrast_d = (\text{ad+bd+cd+abcd-ab-ac-bc-1}) \quad \textbf{(3-5)}$$

$$Contrast_{ab} = (\text{ab+cd+abcd-ac-ad-bc-bd-1}) \quad \textbf{(3-6)}$$

$$Contrast_{ac} = (\text{ac+bd+abcd-ab-ad-bc-cd-1}) \quad \textbf{(3-7)}$$

$$Contrast_{ad} = (\text{ad+bc+abcd-ab-ac-bd-cd-1}) \quad \textbf{(3-8)}$$

A normal probability plot graph was constructed for each response variable to identify the variables producing a significant effect. The significance was quantified by calculating their p-value by analysis of variance.

Regression model analysis

A linear regression analysis model was performed for each response variable.

The regression model coefficients β were calculated in the standard manner (Montgomery, 2001):

$$\hat{\beta} = (X'X)^{-1} X'Y \qquad \textbf{(3-9)}$$

Where $\hat{\beta}$ is a regression coefficients matrix, X is the coded variables matrix and Y is the yield matrix containing the corresponding values of the response variable. The significance of individual variables was evaluated by testing the following hypothesis using the generic method outlined by Montgomery (2001).

H_0: $\beta_1 = \beta_2 = \cdots \beta_k = 0$ (Null hypothesis)

H_1: $\beta_j \neq 0$ for at least one j

3.7 Normal Human Osteoblast Cells Culture Experiment

3.7.1 Sample preparation

Twelve HA coated titanium discs (6 mm, diameter and 0.025 mm, thick) were prepared via –COOH SAM. The SAMs were formed using the methods described in section 3.3 and the HA coatings were formed at 37°C in 1.5 SBF for 5 days. Twelve titanium metal discs were also selected to serve as the control. The twenty four discs were sterilized in 99% ethanol for 30 mins, and then air-dried.

3.7.2 Cell culture

Cell culture studies were performed following the protocols in the previous study of normal human osteoblast (bone) cells (NHBC) proliferating on tantalum metal (Findlay et al., 2004). In this study, NHBC were derived from two different individuals and grown from trabecular bone samples obtained during joint replacement surgery. These were identified as donor-ML and donor-MY, separately. The cells were cultured in air in a humidified incubator containing 10% fetal calf serum (FCS), 0.2mM l-glutamine and ascorbate 2-phosphate at 37 °C with 5% CO_2. Cells were planted on both HA coated titanium discs and uncoated titanium discs in a 24-well plate at a dose of 50 µl containing 2×10^4 cells per well.

3.7.3 Measurement of calcium levels

The number of cells present is assumed to be directly related to the calcium levels of the cell layer. Therefore, by measuring this, the growth in the number of cells may be determined. The calcium level measurements were performed in triplicate at sampling times of four and six weeks. The cultures were first washed three times with Ca^{2+}- and Mg^{2+}-free phosphate buffered silane (PBS). The calcium present in the layer was dissolved by adding 25 ml 0.6 M HCl. Samples from cells grown on the various substrates at the different time points were placed in a 96 well plates. Calcium levels were measured using a colorimetric assay (TRACE Laboratories, Melbourne, VIC, Australia) at 570 nm on a MR7000 microplate reader (Dynatech Laboratories, Guernsey, Channel Islands). Calcium standards at various concentrations were prepared using $CaCl_2$.

4 Results and Discussion

4.1 Introduction

The key goal of this work was to determine conditions to optimize SAM layer formation. Hence, the results of several previous studies were considered and compared. As a consequence, SAMs with four different functional end groups were prepared: $–SO_3H$, –OH, –COOH and $–PO_4H_2$ SAMs. WCAM and TOF-SIMS were used to confirm the presence of SAM layers and demonstrate that the experimental methods were effective and reliable.

The next step was the formation of HA layers onto the titanium substrates containing the SAMs by immersion in SBF. HA layers formed on each SAM surface and on the Ti control wafers. HA layers formed on each functional end group end were analysed and compared by FTIR, XRD, SEM and EDS. A one-half fractional factorial experiment was also designed and performed to explore possibilities to improve the HA coating's growth rate by altering the reaction conditions. Four key reaction parameters were considered: the Ca ion concentration in SBF, the SBF Ca/P ratio, pH and reaction temperature.

Finally, a human bone cell culture experiment was conducted to measure the *in-vitro* performance of HA coated titanium made under the enhanced conditions.

4.2 Characterization of SAMs

Characterization of these SAMs was performed by applying water contact angle measurement and TOF-SIMS.

4.2.1 Analysis of the water contact angle for the various SAMs

Table 4.1 summaries the results of water contact angle for each SAM and the titanium control wafers. The table includes published static water contact angles for Ti, hydroxylated Ti, for the same or similar SAM on Ti, and the same or similar SAM on gold.

Water contact angles measured for Ti and hydroxylated Ti are similar to those reported by Liu et al. (2002) and Niesen et al. (2001) where similar materials and preparation methods were used.

The water contact angle, and hence hydrophobicity of the surface, increased substantially upon introduction of the $–CH=CH_2$ SAM. The values observed were consistent with those measured by Liu et al. (2002). Liu et al. used an identical $–CH=CH_2$ SAM and preparation method.

For the –OH SAM, the water contact angle, and hence hydrophobicity, decreased following the chemical modification of ethyl group (as would be expected). However, the value is higher than that obtained by Liu et al. (2002) whose preparation method was followed.

This value and that of Liu et al. (2002) are both higher than water contact angles reported for the –OH SAMs attached to gold surfaces. Preparation methods for the SAMs on gold were identical to those for titanium, except that the surface does not require hydroxylation and a thiol instead of silane coupling agent is normally employed.

Tanahashi & Matsuda (1997) prepared a –OH SAM on gold. They used an identical C_8 organic spacer, but in their work, the SAM already contained an –OH group on the terminal carbon and subsequent chemical modification was not required. A value of 20^o was obtained. Martins et al. (2003) prepared a –OH SAM in an identical manner but with a slightly longer C_{10} organic spacer. They measured a contact angle of 18^o. However, with

an identical method, Barbosa et al. (2004) obtained a water contact angle of 48^{o}.

There may be a number of explanations for these divergent results. For example, the experimental process may not be exactly reproduced following the method of Liu et al. (2002) The lower values observed with gold may be a function of the substrate type, however, the indirect method involving subsequent modification of a $–CH=CH_2$ SAM may not be as effective as direct application of a SAM containing an –OH functional group. For example, total conversion of the ethyl functional groups may not occur and these groups would remain on the SAM surface, contributing to higher water contact angles.

Alternatively, the –OH may not always add to the terminal carbon during hydration of the $–CH=CH_2$ functional group. Hence, methyl groups may obscure some of the –OH functional groups on the SAM. This might also explain the higher water contact angles measured by Liu et al. (2002) and in this study, when compared to other studies on gold using direct addition of a –OH containing SAM.

In either case, the chemical modification step may not have been as efficient as Liu et al. (2002) However, for the –COOH SAM, which was also prepared by chemical modification of the $–CH=CH_2$ SAM, a lower water contact angle than Liu et al. (2002) was observed. Furthermore, the values were near those obtained for the same or similar –COOH SAMs on gold.

The $–PO_4H_2$ SAM was also prepared by chemical modification of the $–CH=CH_2$ SAM. Measured water contact angles were almost identical to those reported by Liu et al. (2002) However, the value is slightly higher than a value previously reported on gold.

The –OH, –COOH and $–PO_4H_2$ SAMs were all constructed from a single production batch of wafers containing the $–CH=CH_2$ SAM.

The $–SO_3H$ SAM possessed a different organic spacer and was prepared indirectly from a thiol functional group with subsequent chemical reaction with oxone. An identical SAM (except for coupling agent) to Niesen et al. (2001) had been employed to produce a $–SO_3H$ SAM on gold. A virtually identical value to theirs was obtained.

Table 4.1: Measured water contact angles and literature values obtained for the same or similar SAMs with Ti and Au.

Surface	Experimental values				Literature values	
	1	2	3	Ave.	Ti substrate	Gold substrate
Ti	65.1^{o}	68.2^{o}	63.1^{o}	65^{o}	68.3^{o} [1]	n/a
Ti–OH	52.2^{o}	47.3^{o}	44.5^{o}	48^{o}	45^{o} [1]	n/a
SAM–$CH{=}CH_2$	117.8^{o}	115.9^{o}	117.7^{o}	117^{o}	105^{o} [1]	-
SAM–OH	85.3^{o}	84.9^{o}	84.6^{o}	85^{o}	67.7^{o} [1]	48^{o} [4],18^{o} [5],20^{o} [6]
SAM–COOH	24.0^{o}	28.0^{o}	21.3^{o}	24^{o}	48.3^{o} [1]	15^{o} [3],32^{o} [4],32^{o} [5] ,36^{o} [6]
SAM –PO_4H_2	49.1^{o}	48.1^{o}	46.8^{o}	48^{o}	46.8^{o} [1]	36^{o} [6]
SAM–SO_3H	29.9^{o}	30.2^{o}	30.1^{o}	30^{o}	-	33^{o} [2]

1. Liu et al (2002); 2. Niesen et al. (2001).; 3. Scotchford (1998); 4. Barbosa et al. (2004); 5. Martins et al. (2003); 6. Tanahasi & Matsuda (1997).

Whilst considering the water contact angle results, the question arose to whether complete surface coverage by the SAM was achieved? This appears to have been overlooked by previous studies. Clearly, the extent of surface coverage obtained could contribute to observed variations in water contact angle values. For this study, the average water contact angle of hydroxylated titanium was 48^{o}. Poor coverage of this surface with a SAM layer could be expected to cause water contact angles to recede or advance towards this value depending on if they were more hydrophobic or hydrophilic, respectively.

It is not believed that inadequate coverage is a problem with the SAMs that were produced. Like previous studies, it was intended to implicitly measure success of SAM preparation by whether or not a HA layer was obtained. However, the density and distribution of coverage of SAM on a surface could influence the rate and extent of HA formation and resulting properties of the coating.

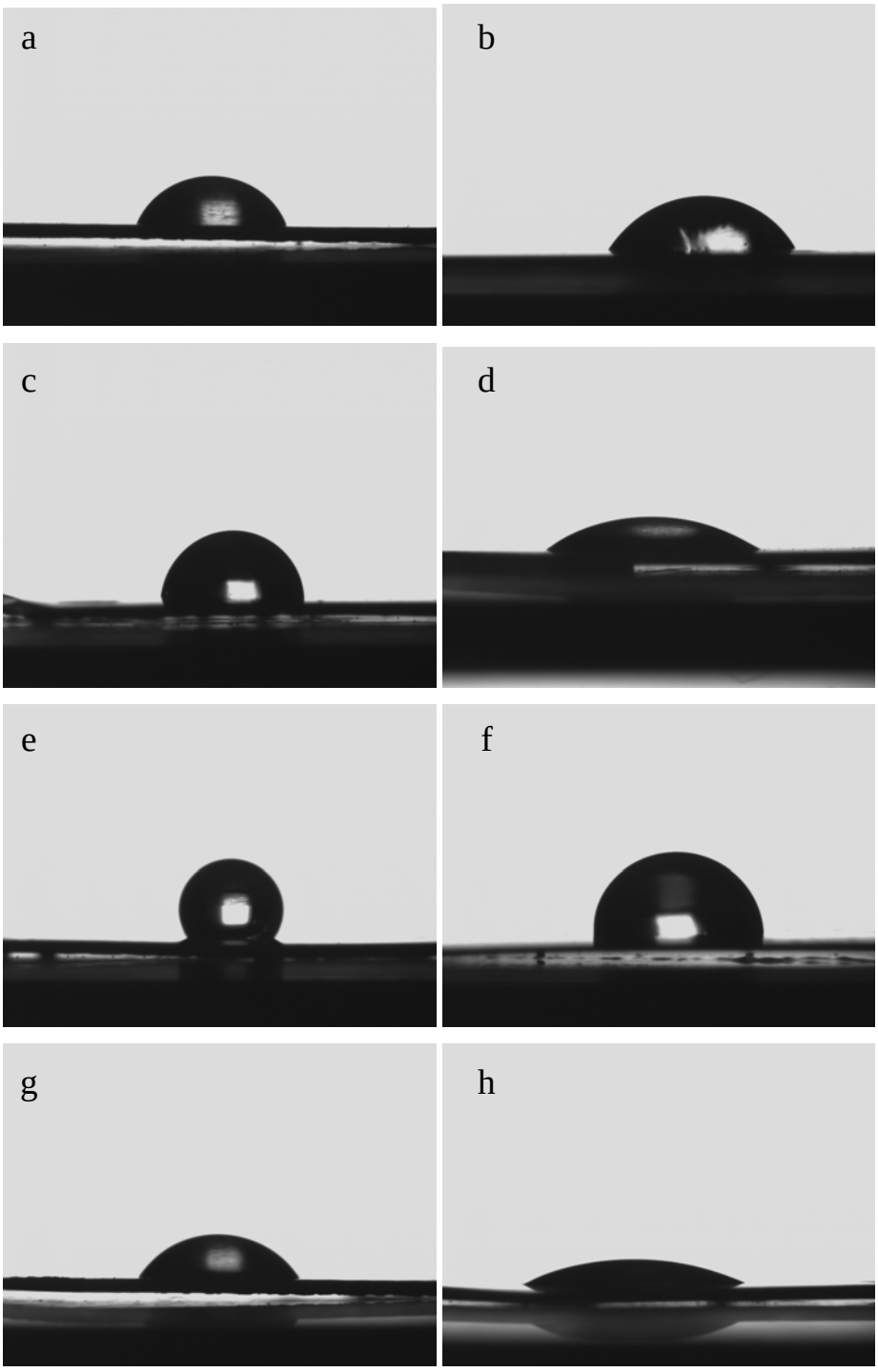

Figure 4.1: Drop images of different SAM surfaces(a) pure titanium; (b) hydroxylated titanium; (c) titanium with –SH SAM; (d) titanium with $–SO_3H$ SAM; (e) titanium with $–CH=CH_2$ SAM; (f) titanium with –OH SAM; (g) titanium with $–PO_4H_2$ SAM; (h) titanium with –COOH SAM.

4.2.2 Results of the TOF-SIMS analysis for various SAMs

Results of TOF-SIMS analyses for the Ti substrate, the hydroxylated Ti and the $–SO_3H$, –OH, –COOH and $–PO_4H_2$ SAMs are summarized in Table 4.2. The data are for a single TOF-SIMS analysis for each surface type, as replication was not possible due to limited equipment access. The table presents elemental ratios of the ion counts obtained by TOF-SIMS for Si, C, O, P and S relative to Ti.

Elemental ratios measured for the pure Ti foil are consistent with a TiO_2 surface layer: the only other major element present is O. However the ratio of O to Ti is higher than the stoichiometric ratio of 2 for TiO_2. This was surprising as the ion beam in TOF-SIMS is believed capable of penetrating the surface to several microns releasing ionic species through to this depth. The thickness of an oxide layer on Ti would only be several nanometers. Therefore, it was expected the ratio might be lower.

TOF-SIMS analysis of the Ti foil also indicated presence of C. Takeuchi et al. (2003) found similar traces of C on untreated Ti foil from analysis by X-ray photoelectron scattering. They attributed the C to natural organic contamination, and this would be a plausible explanation.

Following hydroxylation of the Ti foil, the C contamination disappeared. As expected, hydroxylation does not appear to affect the O/Ti ratio. However, the results indicate that S remains on the Ti surface. Takeuchi et al. (2003) have reported that a S residue will occur on Ti following pre-treatment which involves sulfuric acid. Furthermore, they observed that the S residue was difficult to remove by subsequent washing. It can be observed that the S residue appears to remain even after addition of SAMs onto the hydroxylated surface.

Si and C are detected in TOF-SIMS measurements following addition of each of the SAMs onto the hydroxylated Ti, suggesting that SAM preparation methods were successful. (However, as noted during discussion of water contact angle results, the extent of SAM coverage achieved by each method was not quantified.)

For the –COOH, $–PO_4H_2$, $–SO_3H$ SAMs, there appears to have been increases in the O to Ti ratios, which would be consistent with the contribution of additional O atoms from their functional groups. However, the O to Ti ratio measured for the $–SO_3H$ SAM was higher

than that for the $–PO_4H_2$ SAM, where the opposite might have been anticipated.

As expected, only P was detected for the $–PO_4H_2$ SAM. Likewise, the $–SO_3H$ SAM has a much higher S to Ti ratio than the other SAMs, suggesting the extra S in its functional group is contributing above the S residue that was present on the hydroxylated Ti.

Table 4.2: Elemental ratios obtained by TOF-SIMS of Ti, hydroxylated Ti and different functionalized SAMs.

Ratios	Ti	Ti-OH	SAM-OH	SAM–COOH	SAM–PO_4H_2	SAM–SO_3H
Si/Ti	0.0	0.0	0.2	0.4	0.3	0.2
C/Ti	0.1	0.0	0.6	0.8	0.7	0.4
O/Ti	2.8	2.7	2.6	2.8	3.5	4.5
P/Ti	0.0	0	0.0	0.0	0.1	0.0
S/Ti	0.0	0.2	0.2	0.2	0.3	0.6

Considering both the water contact angle measurement and TOF-SIMS analysis results, the SAMs formation on titanium substrates can be confirmed.

4.3 HA Formation in SBF

The formation of HA coatings was confirmed by FTIR and EDS. The coating's crystallinity was inspected by XRD. The morphology and thickness of the coatings were inspected by SEM.

4.3.1 Effects of gravity on the formation of hydroxyapatite coatings

As mentioned previously, most coatings were formed in supersaturated SBF. As a result, HA precipitated heterogeneously on the surfaces of wafers or homogeneously in solution. Due to sedimentation, the HA crystals formed homogeneously in solution would fall towards the bottom of the container and could deposit on the surfaces of the wafers if wafers were aligned horizontally.

In practice, there was no visible difference observed between the HA coatings formed on wafers aligned vertically or horizontally. The chemical composition of both coatings was similar (Figure 4.2) as determined from the results of EDS analysis. However, their micro-structures were significantly different (Figure 4.2). The coatings formed on vertical wafers were uniform and organized. However, the coatings formed on horizontal wafers were thinner and the surface was dominated by precipitants. Furthermore, simple flushing with a SBF solution appeared to easily dislodge the coating formed on the horizontal wafers.

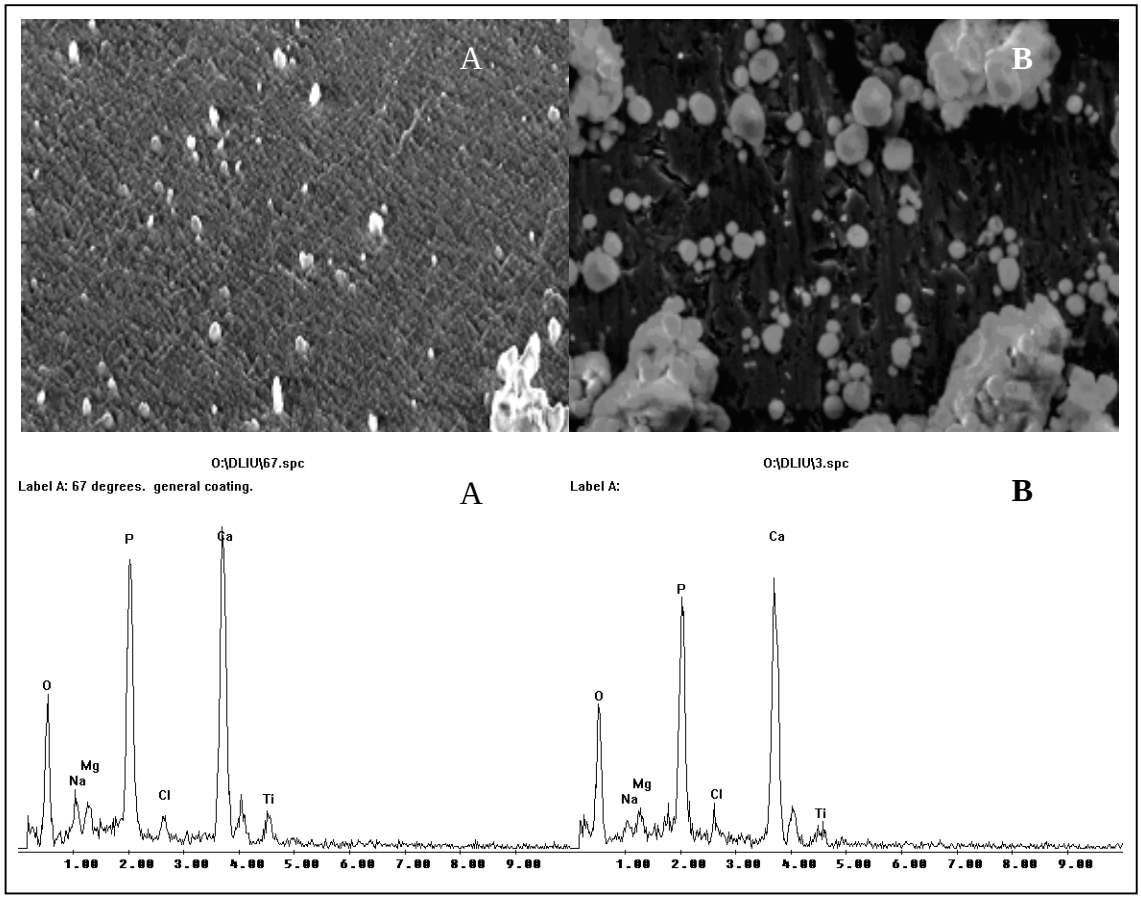

Figure 4.2: SEM and EDS analysis of HA coatings on the wafer oriented (A) vertically and (B) horizontally.

4.3.2 Hydroxyapatite coatings formed on various SAMs

SEM&EDS

The coating thicknesses were measured by scratching the HA layer to reveal the underlying titanium surface and analyzing SEM cross-sections (Figure 4.3). After soaking in SBF for 20 days at 37 °C, the average coating thickness was 1.1 μm for a titanium metal, 1.7 μm for a titanium with –OH SAM, 2.6 μm for a titanium with $–SO_3H$ SAM, 6.3 μm for a titanium with $–PO_4H_2$ SAM and 6.1 μm for a titanium with –COOH SAM.

Values of coating thickness in previous studies using biomimetic HA formation methods varied from 1 μm to 22 μm (Kokubu, 1996; Gu et al., 2004). However, it is difficult to compare because of differences in SBF concentration, the incubation length and substrate type that were used. The sole study reporting the thickness of a HA coating formed on

SAMs was undertaken by Tanahashi and Matsuda (1997). They reported a value slightly larger than 12 μm for a HA coating formed on gold with a –COOH SAM after 30 days' immersion in SBF for at 37 °C.

Figure 4.4 shows SEM images and EDS results for wafer surfaces for Ti with -COOH and $–PO_4H_2$ SAM following 5 day's immersion in SBF. The results of the other SAMs are presented in Appendix A (Figure A3-5). Figure 4.4 includes the SEM image of Ti with the –COOH SAM prior to immersion in the SBF for comparison.

Contrasting the SEM image of the –COOH SAM (Figure 4.4 (C)) with the other images suggests that immersion in SBF has clearly lead to some form of layer depositing on the wafer surface. In each case, the layer appears to have covered the entire of the surface in the field of view. The surface topography of these deposited layers is also very similar to that observed by SEM in other studies (e.g. Liu et al., 2002; Tanahashi & Matsuda, 1997) where HA formation on a SAM or other surface has been observed. In particular, the surface appears to be covered with hemispherical particles on titanium, on $–SO_3H$ and $–PO_4H_2$ SAMs or plate shape crystals on the –COOH SAM approximately seven tenths of nanometers. These crystals are similar to that observed by Tanahashi & Matsuda (1997) using AFM of hydroxyapatite layers formed on a –COOH SAM with gold substrate. The particle mean size of the apatite formed on the titanium, the $–SO_3H$ and the $–PO_4H_2$ SAM is roughly 0.3 μm. However, for the –COOH SAM, the particle size is closer to 0.5 μm.

Figure 4.5 presents the SEM images of Ti and Ti with a -COOH SAMs after soaking in SBF for 30 days. The images of the remaining SAMs are shown in Appendix A (Figure A6-8). Uniform HA coatings with crack-free surfaces were formed on each SAM substrate. However, the HA coating formed on titanium shows a surface full of cracks, some sections are already broken and separated from the surface (Figure 4.5 A1). This is the initial evidence that the use of SAMs may enhance the bonding strength between coatings and substrates.

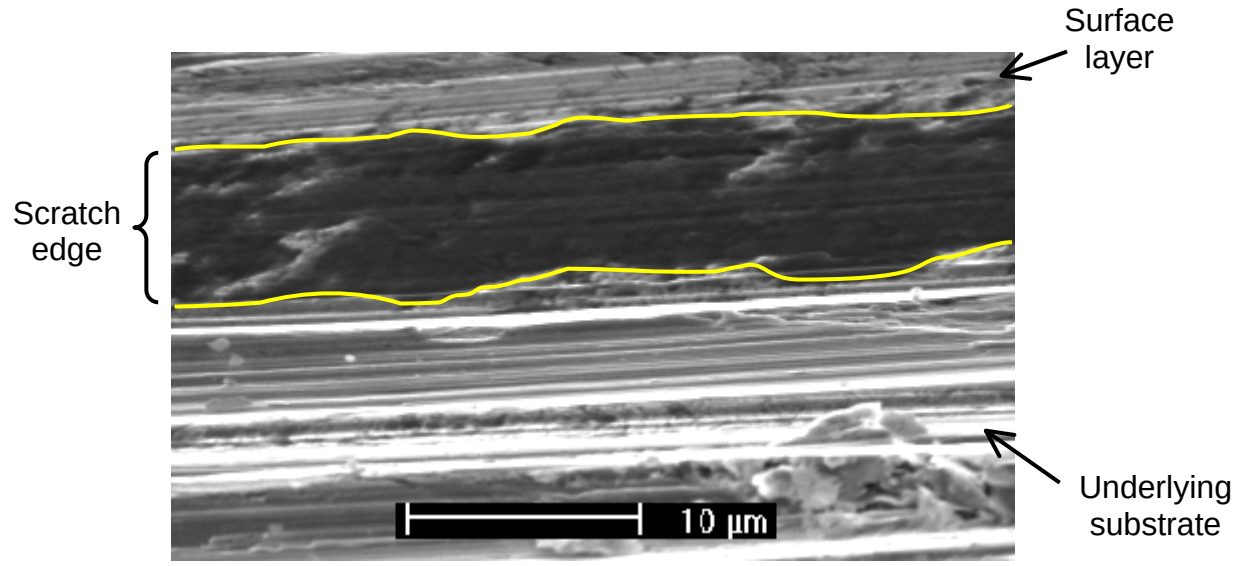

Figure 4.3: Cross section SEM images of HA coatings formed on titanium with –COOH SAM after placing in SBF for 20 days. Note the incident electron beam was tilted by 75°.

Tables 4.3 and 4.4 present the relative mol % of elemental Ca, P, Ti and O and Ca/P ratio obtained for pure Ti and Ti with different SAM layers after 5 and 30 days immersion in SBF.

The high proportion of Ti and O indicate that the underlying surface below the deposited layers dominated the EDS results. However, the presence of Ca and P was detected on all of the wafer surfaces following 5 days' exposure in SBF. These elements were not detected on the Ti wafer with –COOH SAM that was not immersed in the SBF.

These results also suggest that the -COOH SAM appears to have induced HA more quickly than any other SAM based on the percentages of Ca present: -COOH SAM (2.6%) > –SO_3H SAM (1.8%) > –PO_4H_2 SAM (1.7%) > titanium (1.4%) = –OH SAM (1.4%). The ratios of Ca/P followed the order: –COOH SAM (1.22) > –SO_3H SAM (1) > –PO_4H_2 (0.84) > titanium (0.79) ≈ –OH SAM (0.78).

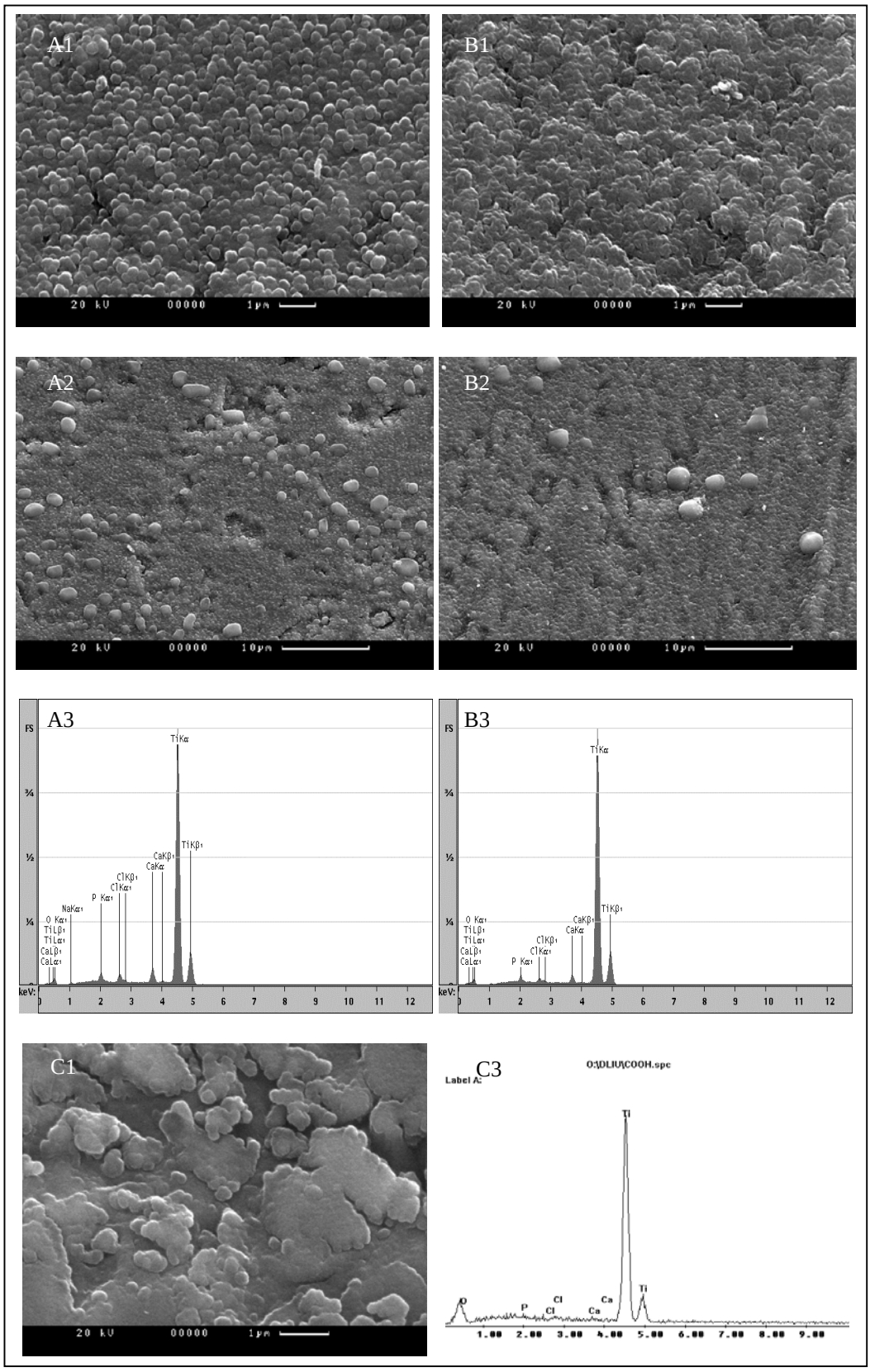

Figure 4.4: SEM images at (1) 1 μm and (2) 10 μm and (3) EDS spectra of HA coating after placing in SBF for 5 days: (A) titanium with $–PO_4H_2$ SAM and (B) titanium with –COOH SAM. (C) is the image of titanium metal with –COOH SAM prior to immersion in

SBF.

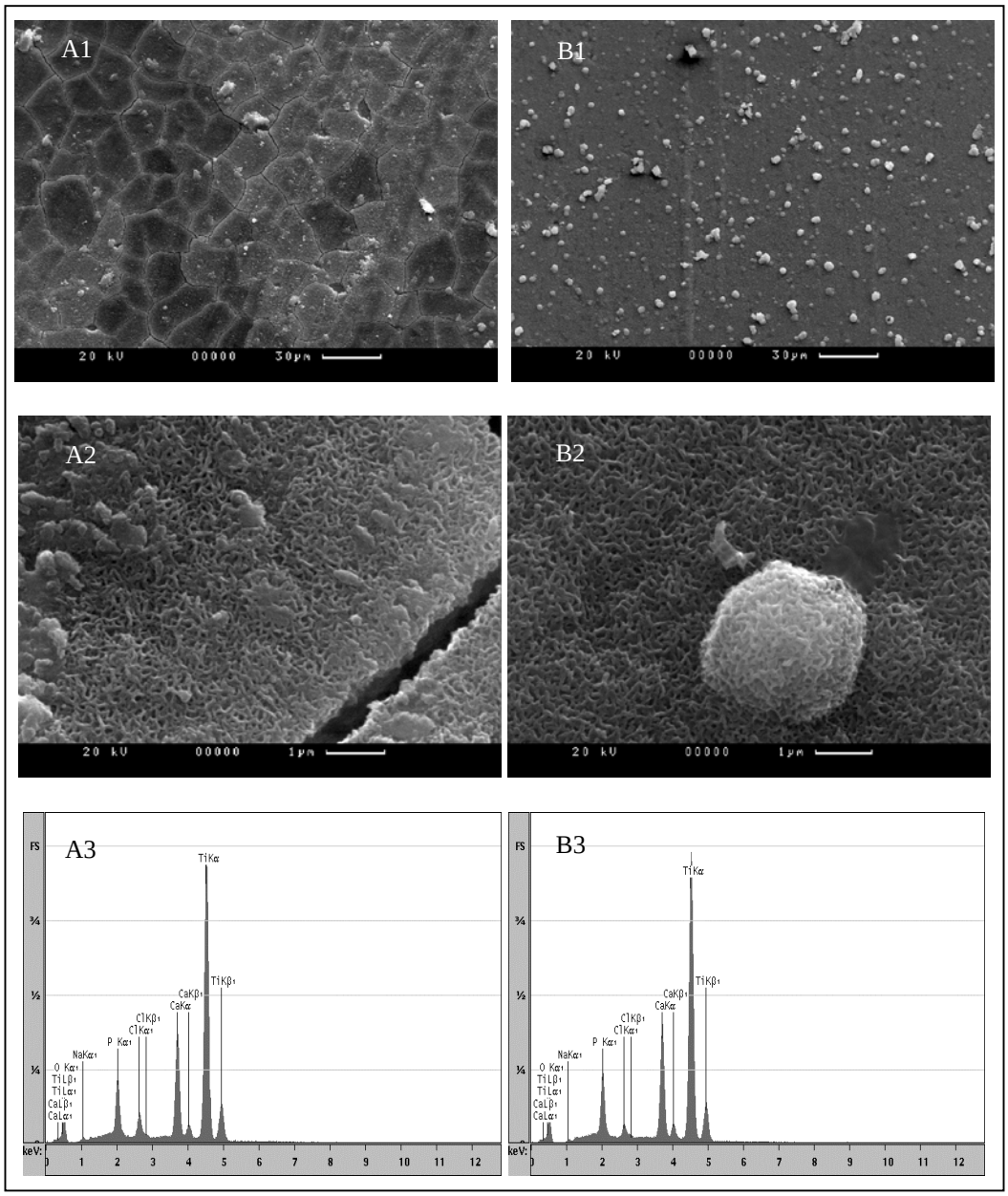

Figure 4.5: SEM images at (1) 30 μm and (2) 1 μm and (3) EDS spectra of HA coating following immersion in SBF for 30 days: (A) titanium metal, (B) titanium with –COOH SAM.

Table 4.3: Elemental compositions (mol %) and Ca/P ratios obtained by EDS of surfaces of pure Ti and Ti with different functionalized SAMs after soaking in SBF for 5 days.

Element	HA coatings formed on different substrates					SAM–COOH
	Ti	SAM-OH	SAM–COOH	SAM–PO_4H_2	SAM–SO_3H	
Ca	1.4	1.4	2.6	1.7	1.8	0
P	1.8	1.8	2.1	2.1	1.8	0
Ti	62.4	62.3	57.5	59.3	59.0	48.25
O	34.3	34.5	37.8	36.9	37.4	51.75
Ca/P	0.79	0.78	1.22	0.84	1	N/A

Table 4.4: Elemental compositions (mol %) and Ca/P ratios obtained by EDS of surfaces of pure Ti and Ti with different functionalized SAMs after soaking in SBF for 30 days.

Element	HA coatings formed on different substrates				
	Ti	SAM-OH	SAM–COOH	SAM–PO_4H_2	SAM–SO_3H
Ca	6.8	9.3	10.3	9.7	9.9
P	4.6	6.1	6.4	6.3	6.1
Ti	39.9	34.5	32.3	31.5	33.8
O	48.7	50.1	51.0	52.4	50.2
Ca/P	1.49	1.52	1.61	1.55	1.62

Comparing the tables 4.3 and 4.4 suggests that the element Ca, P, O and Ca/P ratios increased on every wafer with the incubation time. By contrast, the Ti percentage decreased. This confirms the growth of the HA coatings.

The Ca/P ratios calculated from the EDS results are different for Ti and each of the SAM types. After 30 day's soaking, the values range from approximately 1.49 up to 1.62, with the –COOH and the –SO_3H SAM having the highest Ca/P ratio.

Various Ca/P ratios for crystalline HA are reported in the literature. Higher values in the range 1.6 to 1.7 are common for non-biomimetic techniques, where Ca and P containing materials are directly applied onto the implant surface to achieve a desired ratio. These values are consistent with the theoretical stoichiometric ratio of Ca to P in pure HA, which is 1.67. In human bone, however, the ratio can vary from 1.5 up to 1.62 depending on the type and location of bone (Suchanek and Yoshimuria, 1998). Interestingly, Tanahashi & Matsuda (1997) obtained values ranging from 1 to 1.3 for HA layers formed by immersing gold coated with –COOH and $–PO_4H_2$ SAMs in a SBF. Unfortunately this appears to be the sole study that has reported Ca/P ratios for –COOH and $–PO_4H_2$ SAMs using a biomimetic approach. Kokubo (1996) also reported the Ca/P ratio for SAMs using a biomimetic technique. He measured the ratio for HA layers formed on glass particles coated with various polymers following immersion in SBF. Values in the range 1.36 to 1.52 were obtained. Kokubo attributed the lower values to Ca deficient forms of HA, but did not comment on whether such forms where associated with natural bone.

FTIR

Figure 4.6 presents the Fourier Transform Infrared (FTIR) transmission spectra for pure Ti foil and Ti with each SAM layer following 1 and 10 days immersion in SBF.

The major IR adsorption bands are readily identifiable for HA and occur at (Markovic et al., 2004); 574 and 601 cm^{-1} (both associated with ν_4 PO_4^{3-}); 631 cm^{-1} (OH^-); 962 cm^{-1} (ν_1 PO_4^{3-}); 1040 and 1090 cm^{-1} (ν_1 PO_4^{3-}); 1410 and 1450 cm^{-1} (CO_3^{2-}); and 3572 cm^{-1} (OH^-).

Many of these bands are closely grouped and previous studies (Tadic et al., 2002; Markovic et al., 2004) have found that broad unresolved bands in IR spectra indicate poor crystallinity, whereas increasing sharpness of peaks in the adsorption bands are associated with increased crystallinity. Furthermore, these studies suggest that crystalline HA produces distinct peak splitting at 565/605 and 1070/1150 cm^{-1} (Tadic et al., 2002) and that the sharpness of bands at 631, 601 and 574 cm^{-1} indicate well crystallised HA (Markovic et al., 2004).

Analysis of the spectra for Ti with –OH and $–PO_4H_2$ SAMs suggest that the only major adsorption bands produced by these surfaces following immersion in SBF occured at approximately 600 to 630 cm^{-1} and 1000 to 1100 cm^{-1}. These bands are consistent with the

presence of OH^- and PO_4^{3-} ions. As well, the $-PO_4H_2$ SAM exhibits a broad unresolved band at around 3600 cm^{-1}, indicative of OH^- ion. Nearly all of these bands increased in intensity following 1 to 10 days immersion in SBF. However, none of these spectra appear to exhibit adsorption peaks that could be attributed to CO_3^{2-} ions.

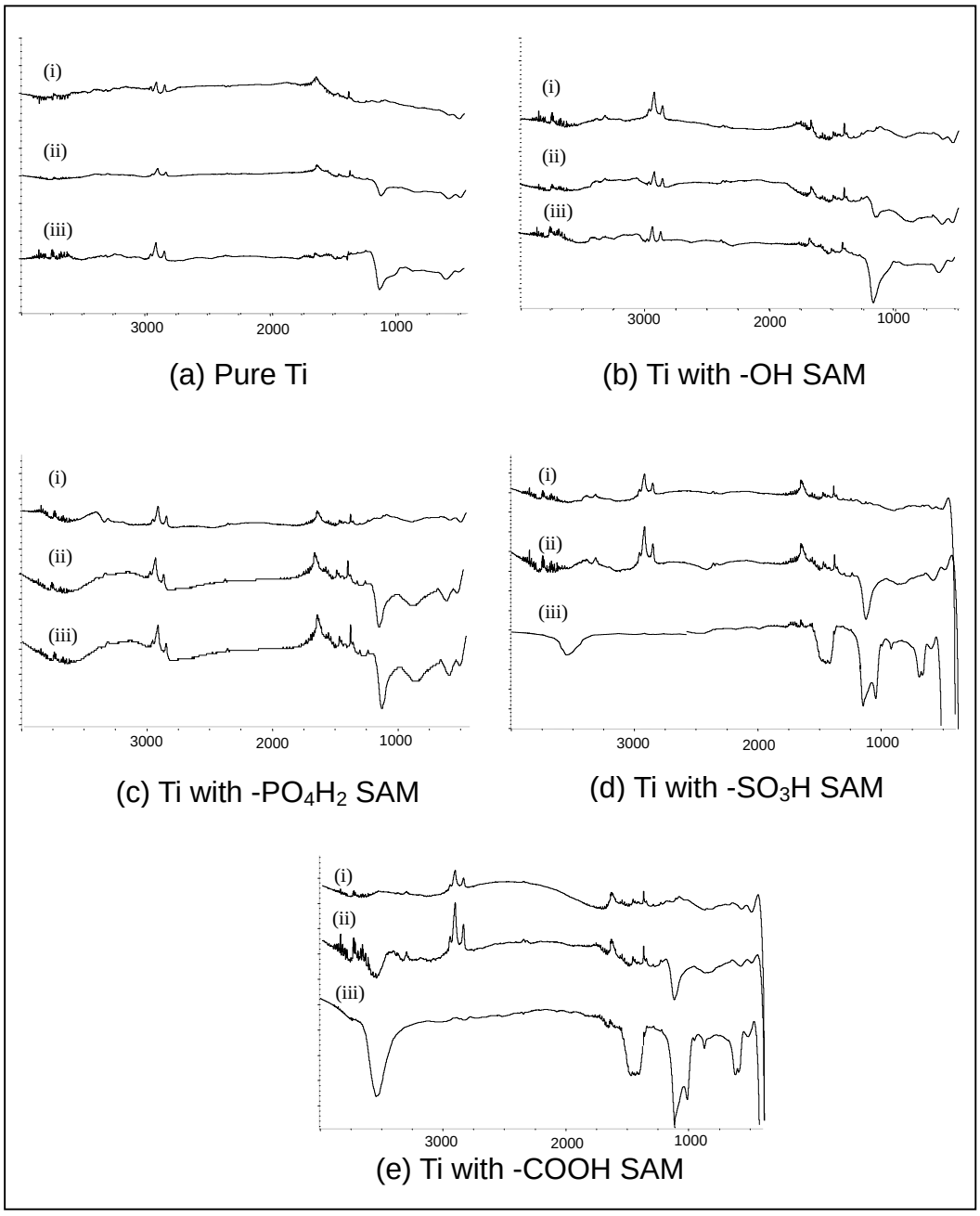

Figure 4.6**:** FTIR transmission spectra of test wafer surfaces after immersion in SBF at (i) 0, (ii) 1 and (iii) 10 days: (a) pure Ti, (b) titanium with –OH SAM, (c) titanium with $-SO_3H$ SAM, (d) titanium with $-PO_4H_2$ SAM and (e) titanium with –COOH SAM.

Spectra for the –COOH and the $–SO_3H$ SAMs display the same adsorption bands as those for Ti and the –OH and the $–PO_4H_2$ SAM. However, additional adsorption bands at 1400 to 1500 cm^{-1}, in a region that indicates the presence of CO_3^{2-} ions (Zhang et al., 2003).

According to Zhang et al.'s (2003) finding, these peaks are features of crystal carbonate HA. This kind of HA is very close to natural bones in both chemical composition and structure. Moreover, Kokubo, (1996) suggested that crystal carbonate HA had a good bioactivity.

Furthermore, the intensity of all of the adsorption bands was higher and with sharper adsorption. The peaks in the bands 600 to 630 cm^{-1} and 1000 to 1100 cm^{-1} are distinctly sharp, and characteristic of the peak splitting associated with crystalline HA.

XRD

Figure 4.7 summarizes the X-ray diffraction (XRD) measurements obtained from the surface of pure Ti and from Ti with different SAMs following immersion in a SBF for 10 days.

Markovic et al. (2004) presents X-ray diffraction data for a synthetic crystalline HA. The major peaks occur at (2θ) angles of 25.9° (associated with a unit cell parameter, hkl, of 002), 31.8° (211), 32.2° (112), 32.9° (300), 35.4° (301) and 39.8° (310).

In the XRD of natural bone (Figure 4.8), the major peaks attributed to crystalline HA lie at approximately 25°, 32° and 40° (Savarino et al., 1993). These peaks are relatively broad indicative of a mixture of amorphous and crystalline HA as well as other contaminants (e.g. protein, collagen, water).

The XRD patterns for both the pure Ti and the Ti with different SAMs include several peaks outside these values at approximately 40°, 43° and 57°. The first two of these can be attributed to Ti and TiO present in the Ti wafers. The origin of the last peak was difficult to determine, however, it is believed associated with the Ti wafer, as it appears in every sample.

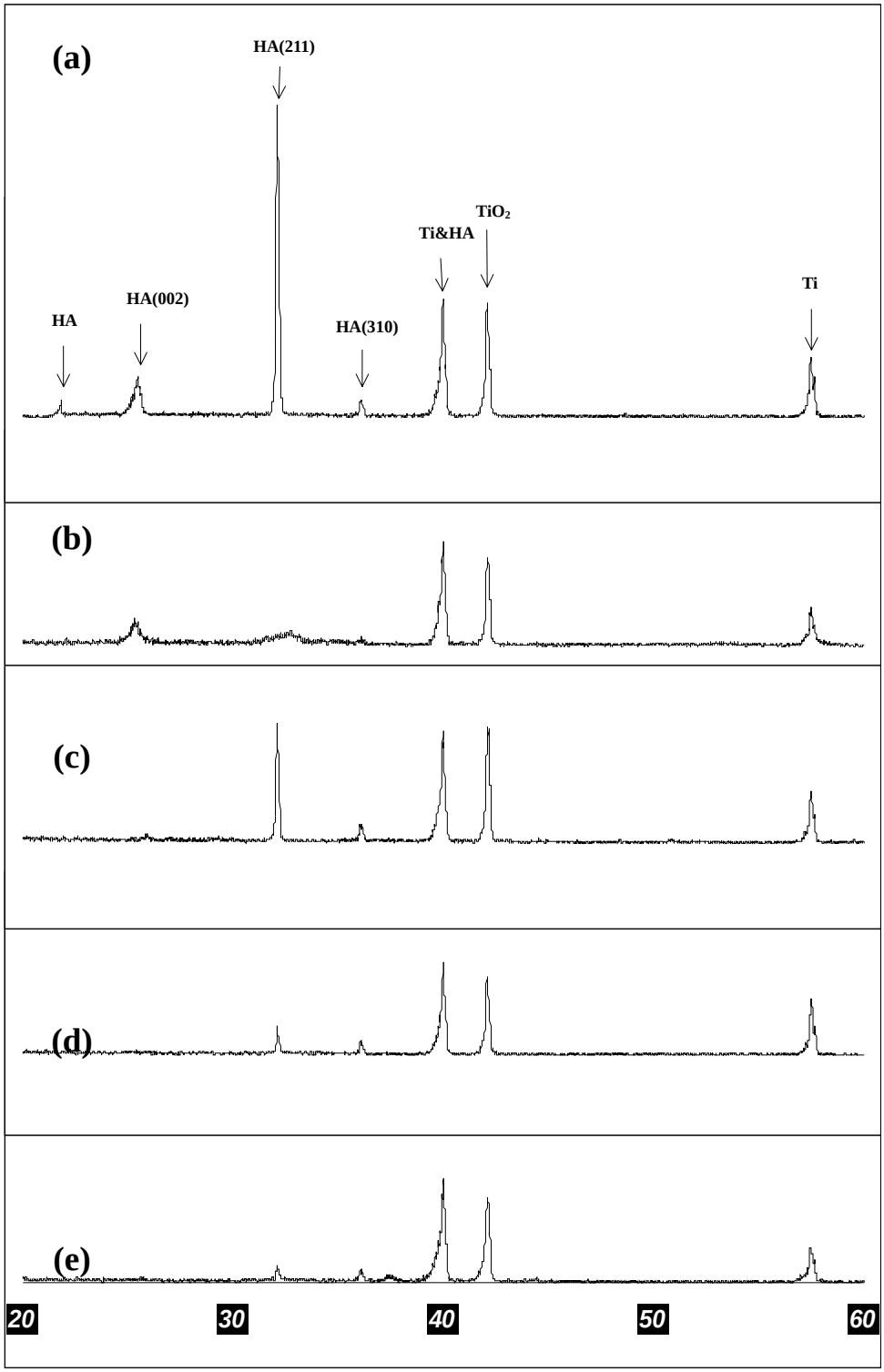

Figure 4.7: XRD analysis results of HA coatings formed on (a) carboxylic acid SAM, (b) phosphate SAM, (c) sulfonic acid SAM, (d) hydroxyl SAM and (e) Ti control.

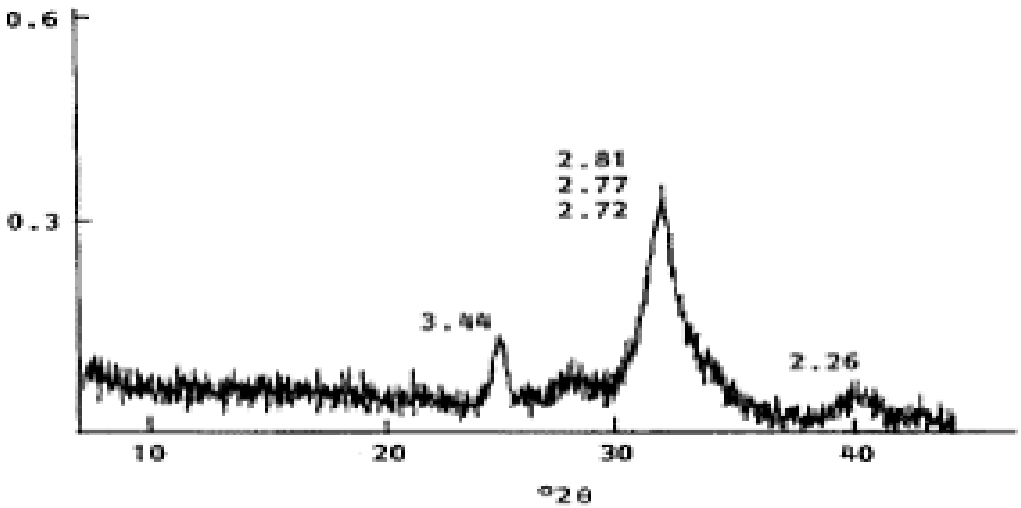

Figure 4.8: XRD analysis of a newly formed bone tissue (Savarino et al., 1993).

The only surfaces to record a substantial peak that could be directly attributed to crystalline HA were the deposited layers formed on Ti with –COOH and $–SO_3H$ SAMs. This peak was located at approximately 32° and occurs in both the synthetic crystalline HA analysed by Markovic et al. (2004) and the aforementioned analysis of natural bone (Savarino et al., 1993). The –COOH SAM a recorded an additional minor peak at 25°, which also appeared in the XRD analysis for the $–PO_4H_2$ SAM. Again, this peak can be found in the analyses of synthetic crystalline HA and natural bone.

These results are slightly different to that obtained by Mao et al. (1998), who prepared a HA layer using a biomimetic technique with a mixed –COOH/–OH SAM on Ti. Interestingly, their XRD pattern produced the major peak at 25° with a smaller peak at 32°.

The key new finding of this study is that the HA coating formed on a carboxylic acid SAM is crystalline and that on a phosphate SAM is amorphous. The reason for this is still not clear. A possible explanation is the different roles played by those functional groups in biomineralization. Bone matrix proteins include type-I collagen (COL-1)-1, osteocalcin (OCN) and bone sialoprotein (BSP)-1. These proteins form the organic scaffold to allow the mineralization of bio- HA (Findlay et al., 2004). Carboxylic acid groups are abundant in these proteins (Weiner, 1982). In contrast, phosphate and sulfonic acid groups appear to be found in mature bone proteins where there is demineralization of the crystal phase (Tanahashi and Matsuda, 1997). These observations may suggest that proteins containing carboxylic acid groups are involved in the crystal-phase formation in bone whereas proteins containing phosphate groups play significant roles in bone healing or remodeling.

4.3.3 Summary of finding on an optimal SAM

In this study, all the substrates tested formed HA coatings on the surfaces. However, the properties of these coatings varied significantly. There were major differences in four key parameters: coating growth rate (thickness), chemical composition (Ca/P ratio), crystallinity and surface morphology.

The -OH SAM was the slowest HA inducer among the four SAM substrates tested. After 20 day's incubation in SBF, the thickness of the coating was approximately 1μm and this value just exceeds that formed on pure titanium. Moreover, the quality of the layer is poor compared to that formed on the other SAMs. EDS confirmed a relatively low Ca/P ratio for this coating (1.52) and XRD indicated a low level of crystallinity.

The $–PO_4H_2$ SAM induced rapid formation of an HA layer. Unfortunately, the coating produced by this SAM was amorphous which will decrease the coating's long-term stability *in-vivo* due to resorption. This problem would significantly limit the application of this SAM.

Coatings produced by –COOH and $–SO_3H$ SAMs are similar in chemical composition and crystal structure. Both SAMs could produce coatings with relatively high Ca/P ratios (1.61 for $–SO_3H$ SAMs and 1.62 for –COOH SAM). XRD and FTIR results confirm highly crystalline products. Moreover, FTIR also showed that the coating formed on the –COOH and the $–SO_3H$ SAMs were carbonated HA as demonstrated by carbonate feature peaks at 1400-1500 cm^{-1}. This form of HA exhibits superior *in-vivo* performance (Dio et al., 1999). However, the HA growth rates on –COOH and $–SO_3H$ SAMs were different. After 20 day incubation in SBF at 37 °C, the coating on –COOH SAM was twice as thick as that formed on the $–SO_3H$ SAMs. Hence, the –COOH SAM is the optimal SAM.

Recent findings (Dowd et al., 2003) about collagen's function in human bone formation may support this conclusion. In their study, the function of osteocalcin, a collagen involved in calcium binding, was investigated. They found that the –COOH groups in this collagen was responsible for the calcium binding. This could be the reason that why the –COOH SAM is superior.

However, the HA formation rate is still relatively low. It would be very interesting to explore ways to improve the speed of coating formation and this provided the prime motivation for the next section of the project.

4.4 Effect of Various Factors on Hydroxyapatite Coatings Formation

A one-half fractional factorial experiment was designed to measure the effects of reaction parameters on the calcium levels and Ca/P ratios of the coatings formed. The results were analyzed by normal probability plots and regression model analysis.

4.4.1 Data collection

EDS analysis results of the one-half fractional factorial experiments are shown in Table 4.5. In this table, the calcium and phosphate ions concentrations of the coatings formed are presented. As well, the calculated Ca/P ratios are tabulated. The calcium content was employed as a surrogate for the growth of coatings. The Ca/P ratio was used as an indicator of the purity of the HA coatings.

Table 4.5: The EDS results of the one-half fractional factorial experiments.

First replicate					**Second replicate**				
	Element concentration (At %)					Element concentration (At %)			
combination	Ca	P	Ca/P	Ca+P	combination	Ca	P	Ca/P	Ca+P
ad	0.97	0.67	1.443	1.64	ad	0.8	0.5	1.6	1.3
bd	0.79	1.84	0.429	2.63	bd	0.91	2.37	0.384	3.28
cd	1.22	1.14	1.07	2.36	cd	1.15	1.07	1.075	2.22
abcd	0.71	1.39	0.511	2.1	abcd	0.3	0.69	0.435	0.99
1	0.44	0.98	0.449	1.42	1	0.25	0.53	0.472	0.78
ab	0.76	1.2	0.633	1.96	ab	1.1	0.94	1.17	2.04
ac	1.42	0.98	1.449	2.4	ac	0.67	0.68	0.985	1.35
bc	0	1.16	0	1.16	bc	0	0.61	0	0.61

4.4.2 Normal probability plot analysis

Figure 4.9 shows a normal probability plot of HA coating's Ca/P-ratio data. The plot suggests variables a (calcium concentration of SBF) and b (SBF's Ca/P ratio) may be significant due to their deviation from the common trend displayed by other data. The

corresponding F values of these two variables from analysis of variance are shown in Table 4.6 and their P-values were less than 0.001.

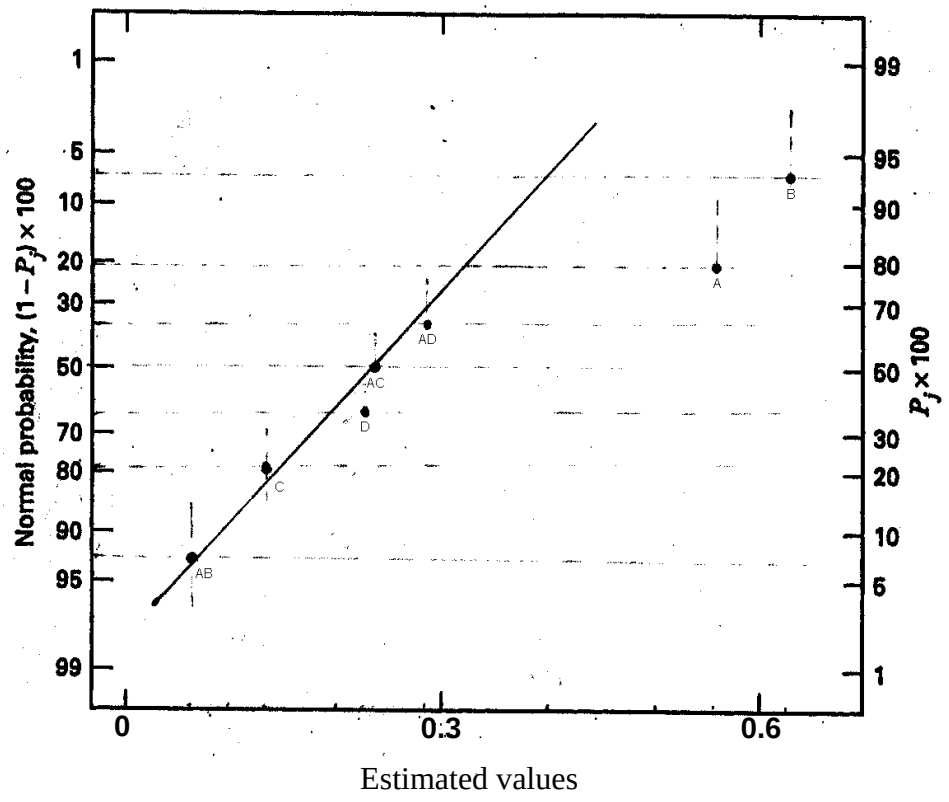

Figure 4.9: Normal probability plot of effects for Ca/P ratio of HA coatings.

Table 4.6: Analysis of variance for factors affecting Ca/P ratio of HA coatings.

variables	Sum of squares	freedom degree	mean square	F	P-values
b	1.553	1	1.553	20.088	< 0.001
a	1.184	1	1.184	15.31	< 0.001
Total	3.742	15			
Error	1.005	13	0.077		

Figure 4.10 presents a normal probability plot of Ca in the HA coating. The scatter of data makes it difficult to accurately draw a line of the best fit, which means that the plot can not exactly recommend which variable has significant effect except the interaction variable ad.

However, this plot still suggests that variables may be divided into three groups according to their positions in the figure. The interaction ad appears to have a significant effect on the calcium content of HA coatings. Variables b, d and a appear to have little effects. Variable c, interaction ac and interaction ad may produce an almost negligible effect. To confirm this statement, it is necessary to measure the P-value for each variable.

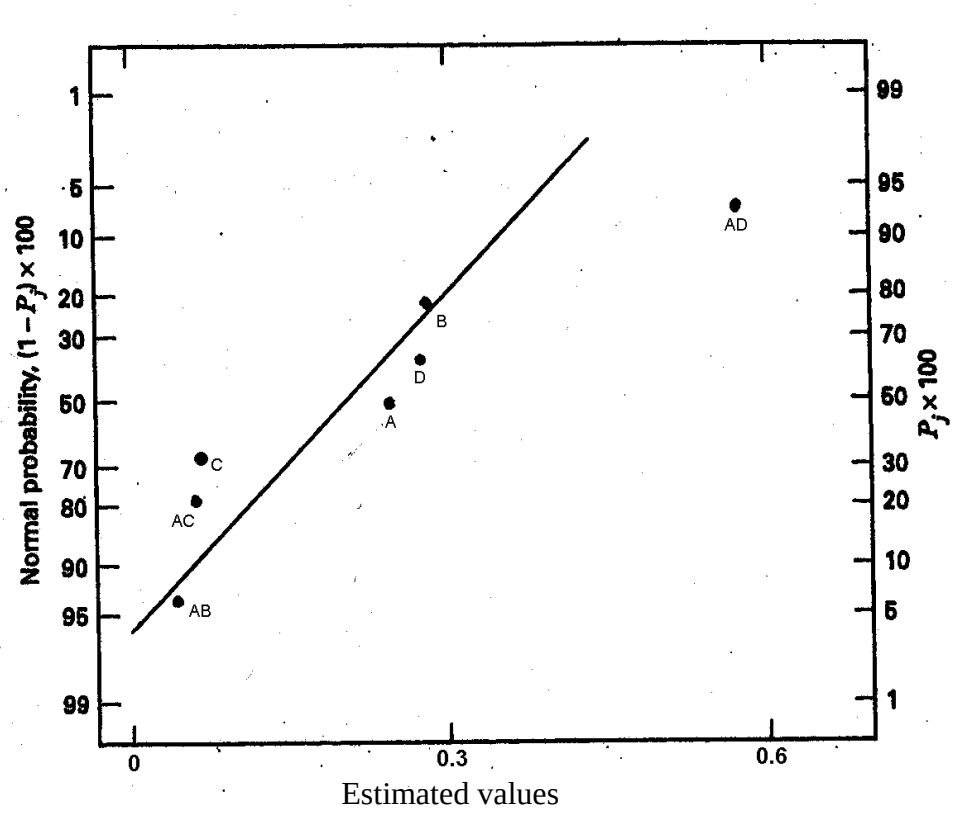

Figure 4.10: Normal probability plot of effects for Ca content of HA coatings.

Table 4.7 shows the F and P values of each variable and their interactions. These values fully agree with the plot results. Interaction ad has the smallest P-value indicating a significant effect. The values of variables b, d and a are less than 0.1. However, the P-values of variable c, interaction ac and interaction ad are too big to be measured based on their F values, which means that they have negligible influences.

Table 4.7: Analysis of variance for factors affecting Ca content of HA coatings.

variables	Sum of squares	freedom degree	mean square	F	P-values
ad	1.293906	1	1.293906	22.25692	< < 0.05
b	0.345156	1	0.345156	5.937146	< 0.05
d	0.305256	1	0.305256	5.250813	< 0.1
a	0.242556	1	0.242556	4.172289	< 0.1
c	0.019044	1	0.019044	0.327582	-
ab	0.016384	1	0.016384	0.281827	-
ac	0.008464	1	0.008464	0.145592	-
Total	2.695844	15	0.179723		
Error	0.465078	8	0.058135		

4.4.3 Regression model analysis

The regression model for Ca/P ratio as

$$\hat{Y}_{Ca/P} = 0.758 + 0.269x_1 - 0.314x_2 - 0.068x_3 + 0.108x_4 - 0.028x_1x_2 - 0.114x_1x_3 - 0.141x_1x_4 - 0.006x_5 \quad \textbf{(4-1)}$$

Regression statistics are presented in Table 4.8. The regression was highly significant.

Table 4.8: Analysis of variance for significance of Ca/P ratio model.

Source of variation	Sum of squares	Degree of freedom	Mean squre	F_0	R^2
Regression	3.542554	8	0.442819	11.54506	0.929549
Error	0.26849	7	0.038356		
Total	3.811044	15			

Analysis of individual regression coefficients is presented in Table 4.9.

Table 4.9: t values of Ca/P ratio variations.

Variables	β	t_0	P-values
Constant	0.758	-	-
a	0.269	5.502053	< 0.001
b	-0.314	-6.42129	< 0.001
c	0.068	-1.39157	< 0.5
d	0.108	2.208481	< 0.1
ab	-0.028	-0.57456	< 0.8
ac	-0.114	-2.33624	< 0.05
ad	0.141	-2.8724	< 0.05
Blocks	-0.006	-0.11499	-

Variables a, b, d, ac and ad were significant, suggesting that Ca/P ratio in HA coating was affected by Ca/P ratio, calcium ion concentration and temperature in the SBF and there were interactions between Ca/P ratio in SBF and pH, and Ca/P ratio in SBF and temperature.

The regression model for the effect on calcium has been developed and presented below.

$$\hat{Y}_{Ca} = 0.718 + 0.123x_1 - 0.147x_2 - 0.034x_3 + 0.138x_4 + 0.023x_1x_2 - 0.032x_1x_3 - 0.284x_1x_4 + 0.071x_5 \quad \textbf{(4-2)}$$

Regression statistics are presented in Table 4.8. The regression was highly significant.

Table 4.10: Analysis of variance for significance of the Ca ion concentration.

Source of variation	Sum of squares	Degree of freedom	Mean square	F_0	R^2
Regression	2.3104	8	0.2888	5.244864	0.857023
Error	0.385444	7	0.055063		
Total	2.695844	15			

According to t test results (Table 4.11), the Ca/P ratio and calcium ion concentration of

SBF and temperature affect the level of calcium in the HA coatings. As well, the interaction between the Ca/P ratio and the temperature influences the response yield.

Table 4.11: t test values of Ca content variations.

Variations	β	t_0	P-values
Constant	0.718	-	-
a	0.123	2.09896	< 0.1
b	-0.147	-2.50392	< 0.05
c	-0.034	-0.58609	< 0.8
d	0.138	2.254671	< 0.1
ab	0.023	0.394221	< 0.8
ac	-0.032	-0.54347	< 0.8
ad	-0.284	-4.84794	< 0.002
Blocks	0.071	1.203972	-

4.4.4 Discussion

Both analysis methods produced similar results. The Ca ion concentration, the Ca/P ratio in SBF solution and the temperature significantly affect the HA coating's Ca content and Ca/P ratio. As expected, a high Ca ion concentration in SBF and temperature could increase the HA coating's Ca content and Ca/P ratio. This may be explained as follows. Higher Ca ion concentration in SBF increased the degree of supersaturation, which could improve the HA coating formation. The effect of temperature may be caused by the changes in the solubility product. In particular, the K_{sp} of HA decreases with an increase in temperature (Gregory et al., 1970), which would increase the supersaturation degree of SBF and, further, the HA coating formation. However, surprisingly, the Ca/P ratio of SBF had negative effects on both HA coating's Ca content and Ca/P ratio. In this experiment, an increased SBF Ca/P ratio was achieved by decreasing the phosphate concentration. It is possible that phosphate concentration is another potential factor but this was not considered in the experimental design. This could cause the abnormal experiment results. However, the exact reason still remains unclear.

The results suggest that to accelerate HA formation (i.e. implied from calcium content) and, at the same time, retain coating quality (i.e. a Ca/P ratio consistent with natural bone) may be achieved by increasing calcium concentration in the SBF and high temperature. As the effect of Ca/P in SBF is unclear, it would be better to keep it constant at the standard SBF ratio of 2.5 until further study is taken.

4.4.5 Enhancement of the HA coat formation

The aim of this experiment was to confirm the possibility of improving HA coat growth rate by altering the reaction conditions based on the results of the screening experiment.

The experiment was performed at high SBF calcium concentration and temperature. If the chosen values were too high, precipitation would occur in the solution before the wafers were immersed in. Therefore, the values for calcium concentration in the SBF and the temperature were within the values used in one-half fractional factorial experiments. By doing this, comparation can be made without risking any instability in the SBF.

The new reaction conditions were at 67 °C in 1.5 SBF (calcium concentration 3.75mM at a Ca/P ratio of 2.5) for 5 days. The conventional conditions as control were 37 °C in standard SBF (calcium concentration 2.5mM with a Ca/P ratio of 2.5) for 5 days (data from the experiments in section 4.3.2). The substrate was titanium with a -COOH SAM.

The coatings formed under conventional conditions have been characterized in section 4.3.2 as crystalline calcium deficient apatite.

The coatings formed at new conditions were characterized using SEM & EDS, FTIR and XRD.

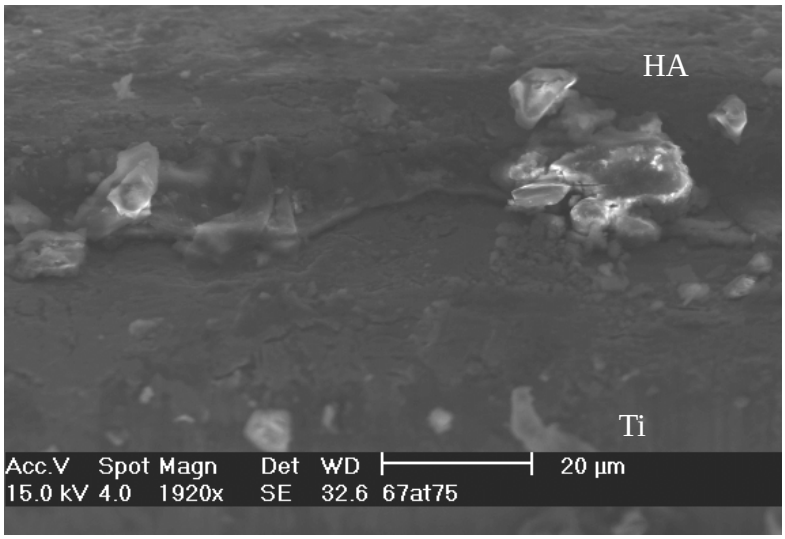

Figure 4.11: Cross section SEM images of HA coatings formed on titanium with –COOH SAM under optimized conditions. Note the incident electron beam was tilted by 75°.

Figure 4.11 shows a cross view of the HA coating formed at the new conditions after 5 days. The thickness of this coating was approximately 12 µm. This value is much greater than that formed using the conventional conditions and an identical incubation period (less than 1 µm). The coating was twice as thick as that formed under conventional conditions following 20 days immersion (6 µm). This result confirmed that new reaction conditions significantly improved HA growth on a SAM coated titanium wafer.

Figure 4.12 compares the EDS results from the two coatings. For the coating formed under conventional conditions Ti element dominated the chemical content. By contrast at the new conditions, the major components in the surface were calcium and phosphate confirming HA growth had been improved under new conditions.

Table 4.12 summarizes the EDS results. The calcium content of the coating produced at new conditions is approximately 6 times higher than that for the layer formed under conventional conditions.

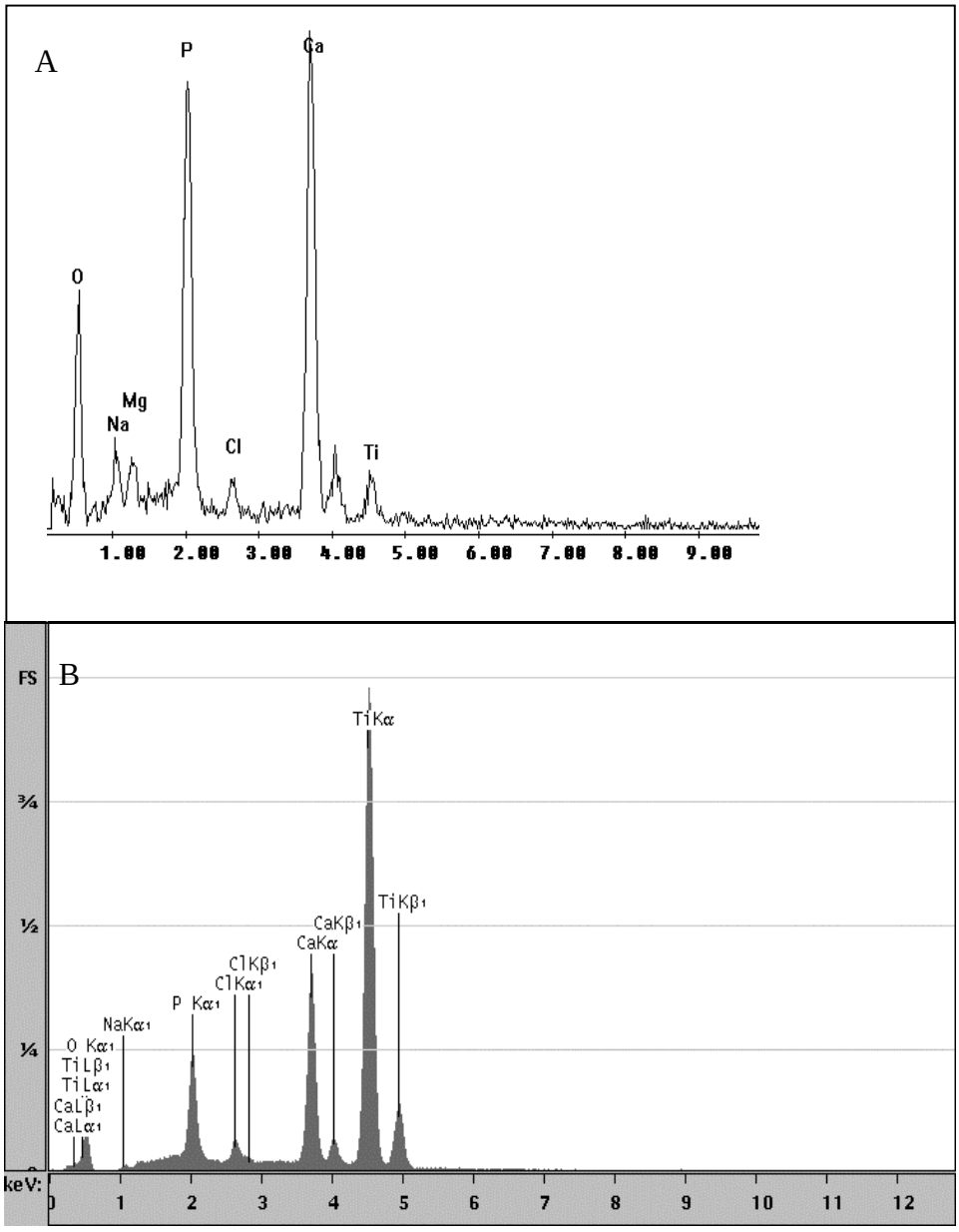

Figure 4.12: EDX analysis of HA layer formed on carboxylic acid SAM (A) in 1.5 SBF at 67 °C and (B) in SBF at 37 °C for 5 days.

Previously, the conventional conditions were chosen to mimic the human body's environment. Concerns were expressed that higher temperatures and calcium ion concentration might significantly increase the degree of supersaturation. Consequently, homogeneous nucleation would overwhelm heterogeneous nucleation and the purity of the coating would decrease. However, as demonstrated in this study, this concern was not realised. After 5 days' immersion in SBF, new conditions increased the Ca/P ratio to 1.3 when the conventional conditions achieved a value of 1.2 at the same time (Table 4.3) but less than 1.6 achieved under conventional conditions after 30 days' immersion in SBF (Table 4.4). Considering the huge difference in incubation time, this could not proof that

the new conditions degraded the HA coating's quality.

Table 4.12: Chemical composition of (A) -COOH SAM soaking in optimized conditions (1.5 SBF at 67°C for 5 days) and (B) -COOH SAM soaking in conventional conditions (SBF at 37°C for 5 days).

Elements	At%	
	A	B
P	11.65	2.05
Ca	15.79	2.48
Cl	1.2	1.47
Ti	1.77	55.27
Na	4.07	2.34
O	63.57	36.39
Mg	1.95	0

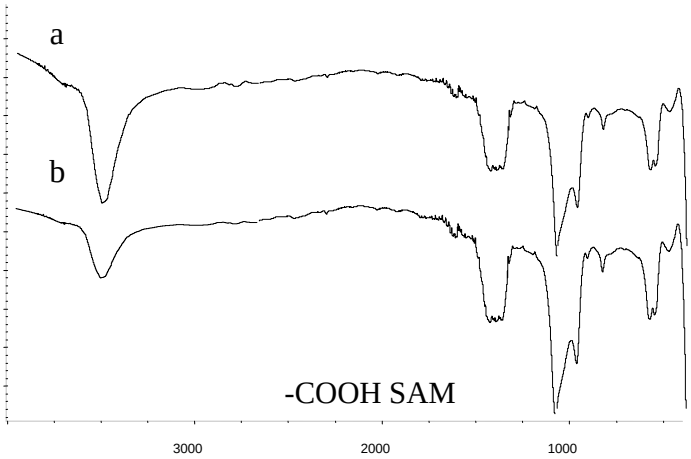

Figure 4.13: FTIR results for HA coatings formed at (a) conventional conditions for 5 days and at (b) new conditions for 5 days.

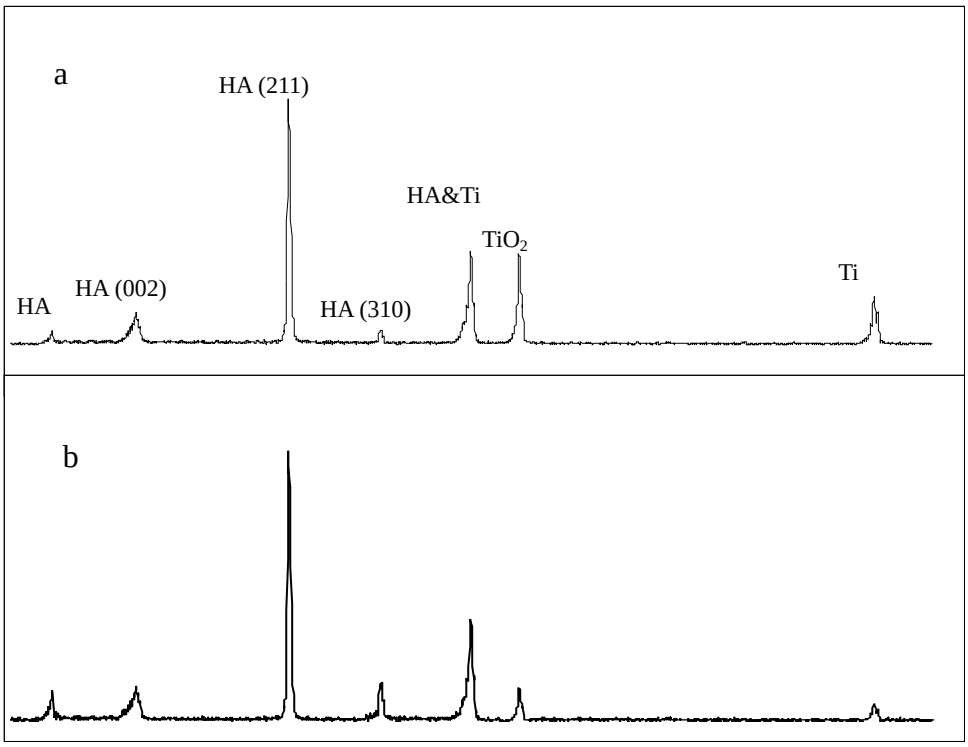

Figure 4.14: XRD results for HA coatings formed at (a) conventional conditions after 5 days and at (b) new conditions for 5 days.

According to Figures 4.13 and 4.14, there was no significant difference in chemical composition and crystallinity between the HA coatings formed in the new conditions and the conventional conditions.

FTIR results (Figure 4.13) confirm that both coats posses major HA character peaks at approximately 600 to 630 cm^{-1}, 1000 to 1100 cm^{-1} and around 3600 cm^{-1}. These bands are consistent with the presence of OH^- and PO_4^{3-} ions. By contrast, the HA coating formed at the new conditions produced higher peaks at 600 to 630 cm^{-1}, 1000 to 1100 cm^{-1} and a smaller peak at around 3600 cm^{-1} when compared with that formed using the conventional conditions.

Both coatings produced similar XRD patterns. The major HA character peaks at 25°, 32° and 40° (2θ) are observed in each pattern. Pattern b displays HA peaks at 22° and 35° exceeding those from pattern a. As well, the Ti peaks present at 43° and 57° on pattern b are smaller than the corresponding peaks for pattern a.

In summary, the new conditions clearly improved the HA coating growth rate with no apparent diminution in coating quality.

4.5 Normal Human Osteoblast Cells Culture Experiment

A surface's potential for biocompatibility may be assessed by the rate of osteoblast proliferation measured by *in-vitro* cell culture experiments. The cell growth rate during these experiments is usually inferred from Ca content caused by mineralization produced by the cells. The Ca content is measured by a standard assay method.

4.5.1 The Standard curve for Ca^{2+} concentration for the mineralization assay

Figure 4.15 summarizes the standard calibration curve obtained for calcium ion concentration versus absorption at 570 nm.

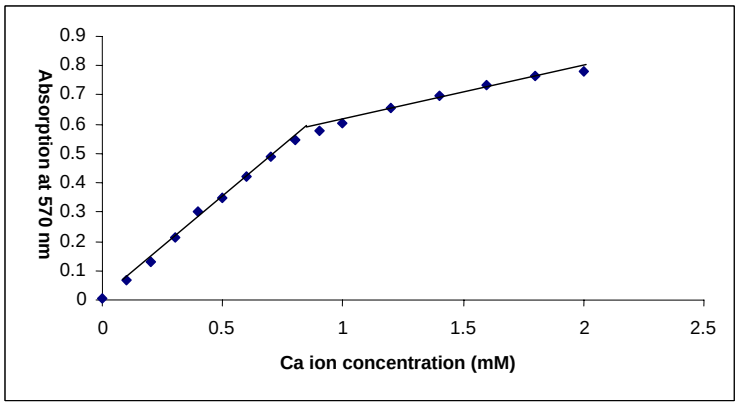

Figure 4.15: Standard curve of Ca concentration.

4.5.2 Measurement of calcium levels

The calcium concentrations in cell layers are summarized in Figure 4.16.

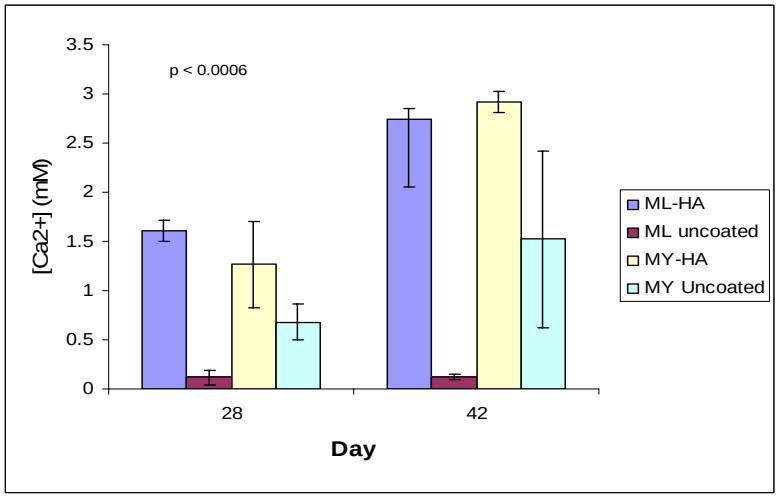

Figure 4.16: Calcium concentrations on coated and uncoated Ti substrates after cell culture for 4 and 6 weeks.

Previous measurements showed that the calcium content in the HA coating on the titanium disc would not affect the result accuracy when measuring the calcium level in the cell layers. Control experiment showed that when a titanium wafer (6mm diameter) with HA coating (12 μm thick) was placed in 25 ml 0.1 M HCl solution, only 0.0045 mM calcium was detected. This is consistent with the theoretical calculation value, 0.0041 mM, which was calculated by the equation 4-3. Considering the values after cells culture, this value was negligible.

$$C_{(Ca)} = [(T \times A \times \rho)/M]/L \qquad \textbf{(4-3)}$$

Where C is concentration, T is coating thickness, A is sample surface area, ρ is the density of HA, M is HA's mole of weight and L is the liquid volume.

After 28 day of culturing, the calcium concentrations on coated titanium substrates are significantly higher than those on uncoated discs. The highest calcium value of coated substrate reported by both donor cells reached approximately 1.7 mM.

After 42 day of culturing, the difference between the calcium concentrations on HA coated titanium and bare titanium was increasingly significant. The average calcium value of coated titanium was 2.8 mM whilst that of bare titanium was 0.87 mM.

Comparing with those of some well recognized biocompatible materials previously measured under similar conditions: 0.13 for CoCr and 0.1 for polished Ta (Findlay et al., 2004), it may be concluded that HA coated titanium has enhanced biocompatibility, although donor-dependant differences were seen.

5 Conclusion

This research has confirmed the potential of SAM techniques for improving the HA formation on titanium metal substrates. The HA formed on negatively charged SAMs grows more quickly and the quality is significantly higher than that grown on bare Ti substrate. Among the SAMs tested, $–PO_4H_2$ SAM and –COOH SAM induced HA formation quicker than any other SAM observed by other researchers. However, the coatings formed on $–PO_4H_2$ SAM were amorphous. Amorphous HA is not stable in human body environment and will dissolve within days after implantation. By contrast, the coating formed on -COOH SAM was characterized as crystalline calcium deficient HA with a chemical composition and a crystal structure close to natural bone. The crystalline phase is believed to remain stable following implantation. The fact that the chemical composition and crystal structure are close to that of natural bone suggested that good bio-performance could be achieved. However, the coating's growth rate on –COOH SAM under normal reaction conditions (SBF, 37 ^{o}C and pH = 7.4) was slow. This low growth rate could limit the industrial application of this technique. To improve the rate of the HA layer formation, the effect of reaction conditions on coating's growth were studied. Calcium concentration, Ca/P ratio and reaction temperature of the SBF produced a significant influence on HA formation. At elevated Ca concentration and temperature, the HA coating formed grew significantly quicker than that under the normal conditions.

In-vitro studies with Osteoblast cells confirmed HA coated titanium via –COOH SAM exhibited superior biocompatibility and osteoconductivity to titanium

This study has produced significant improvements for coating HA on titanium with SAMs. Despite this success, several areas of significance have not been addressed in this work. These areas are summarized as follows:

- The bonding strength between the HA coating and titanium substrate is a key variable. This parameter has not been measured in this study. It has been widely accepted that biomimetic methods can improve the bonding strength and a significant body of literature supports this statement. However, a quantitative study should be undertaken.

- Further work is required to define the necessary thickness of a coating. Such research should be directly related to the environment of the proposed use. The requirements may vary according to the implant purpose and location in the body.

- Current HA formation enhancement experiments performed in this study may only be regarded as screening experiment, which means only trends were observed and accurate optimal conditions still remain unknown. A more comprehensive experimental program is required.

- Finally, although this study has shown that the human bone cells growth may be correlated to the calcium content levels, it would be desirable to measure cell proliferation and the number of cells adhering to the substrate. Quantification of these two parameters would be persuasive when determining a material's biocompatibility and osteoconducty.